LA-8223-MS

Informal Report

2

# Space Nuclear Reactor Power Plants



LOS ALAMOS SCIENTIFIC LABORATORY
Post Office Box 1663 Los Alamos, New Mexico 87545

This report was not edited by the Technical Information staff.

This work was supported by the US Department of Energy, Division of Advanced Nuclear Systems and Projects.

LA-8223-MS
Informal Report
UC-33
Issued: January 1980

# Space Nuclear Reactor Power Plants

D. Buden
W. A. Ranken
D. R. Koenig



CONTENTS

# SPACE NUCLEAR REACTOR POWER PLANTS

by

D. Buden
W. A. Ranken
D. R. Koenig

ABSTRACT

Requirements for electrical and propulsion power for space are expected to increase dramatically in the 1980s. Nuclear power is probably the only source for some deep space missions and a major competitor for many orbital missions, especially those at geosynchronous orbit. Because of the potential requirements, a technology program on space nuclear power plant components has been initiated by the Department of Energy. The missions that are foreseen, the current power plant concept, the technology program plan, and early key results are described.

## I. POTENTIAL MISSION REQUIREMENTS[1]

When the Space Transportation System (STS) becomes operational we will enter a new era in space exploration and exploitation, one that will lead to increasingly complex large space satellites. Many of the great advances in space we have seen to date will be like the early biplanes compared to today's 747 jet liners. There are a number of key technologies emerging that will make this new era feasible, including new approaches of meeting vastly increased demands for power. Large quantities of electrical power will be needed for both sensors and propulsion. Since we will be discussing the potential use of nuclear power, we will concentrate on those areas that appear most attractive for nuclear power, i.e., high-power satellites in geosynchronous orbit and electric propulsion systems for both orbital transfer and planetary exploration missions.

### A. Potential Security Applications

To understand why we consider reactors a necessity for space electrical power, one should have an understanding of the role space will play in future national defense. The statement -- "take the high ground and hold it" -- is recognized as axiomatic in defense. But, where will the "high ground" be in the future? In feudal times when swords were the dominant weapon, the castle ramparts were the "high ground." In World War II, the airplane became the "high ground." Now, the "high ground" has shifted to space. This upward mobility of the "high ground" tends to be an evolutionary process. For example, the airplane in World War I was an extension of the ground forces used mainly for improved surveillance, but slowly evolved to being a mobile artillery piece. During World War II the airplane came into its own, ranging far and wide as a strategic attack force as well as providing cover for ground and naval forces. The airplane provided a means of destroying the war manufacturing capability of an enemy without occupying the immediate territory. Air power starting as an evolutionary force, added a new dimension to attack applications, and later provided a revolutionary addition to defense tactics.

Today, space is in an evolutionary phase, but by the end of this decade it will become the "high ground" for defense. Currently, space is being used as an extension of our terrestrial forces, providing

improved communications, navigation, and surveillance. This function is being performed as an extension of existing systems. The Space Shuttle and new technologies now emerging will soon provide a new force and defense capability that will be revolutionary. This move to space can provide the ability to observe any location on the earth, defeat enemy long range missiles, defend space facilities, and provide instantaneous world-wide communications, command, and control. We may see space become a unified command with the elements organized much like a carrier task force, air wing, or army division (Fig. 1). In this Space Command structure large radars, optical and laser surveillance devices will be used to observe all locales on the earth's surface no matter the weather and to even penetrate the oceans. No large-scale military maneuvers will be possible without being observed. Communications will be instantaneous on a world-wide basis. Using space, we will be able to support or to provide satellite defense, destruction of enemy satellites, and destruction of enemy missiles. The possibilities also exist that we may even attack targets within the atmosphere, such as bombers or cruise missiles. These elements may all be unified by command centers located in space.

The USSR has already implemented many of the elements of a future space force including a continuously manned and resupplied space station. They have very active programs in space and a demonstrated anti-satellite capability. Table I lists their military payloads through 1975, while Fig. 2 shows the number of successful launches with no indication of a slackened pace since then. Examination of Table I shows a significant surveillance effort. "Military Recoverable Observation" was used extensively by the Soviets during the 1973 Yom Kippur War where Kosmos 596, 597, 598, 599, 600, 602, and 603 were used to monitor the battles below. Other Kosmos were used to monitor the cease-fire agreement compliance.

In order for the US to accomplish its revolutionary move to space, large and varied power systems will be required. Satellites, including the power systems, will need to be hardened and made survivable against enemy attack. Surveillance, navigation, and communication devices will require a few kilowatts up to perhaps one hundred kilowatts operating over a 5-10 year period. Solar arrays with batteries will continue to be a prime power source. However, radioisotopes will become a major

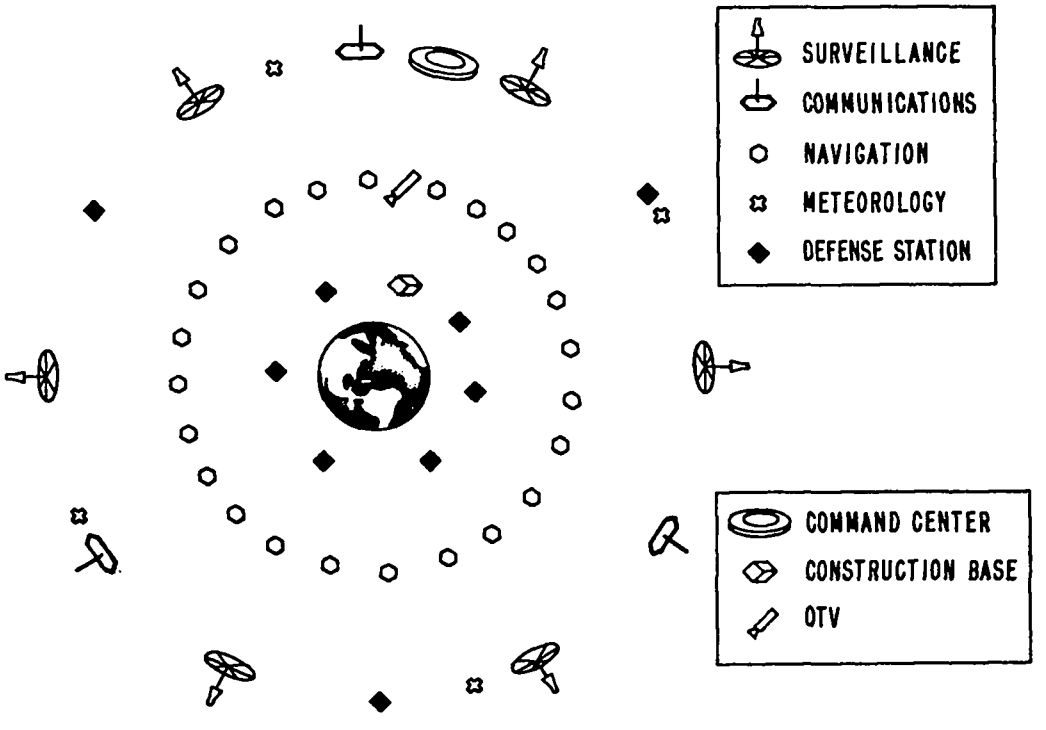


Fig. 1. Space command.

TABLE I

SUCCESSFUL MILITARY PAYLOADS

TOTALS 1957-1975 FOR U.S.S.R-U.S.*

| MILITARY PAYLOAD | U.S.S.R. | U.S. |
|---|---|---|
| Military recoverable observation | 328 | 220 |
| Minor military (environmental monitoring, radar calibration, electronic ferret) | 94 | 90 |
| ELINT, FERRET (Satellite picks up electronic signal, communications, and radar intelligence) | 42 | 0 |
| Navigation and Geodesy | 46 | 31 |
| Military communications, store-dump | 128 | 0 |
| Early warning satellites (senses and transmits electromagnetic signals of nuclear explosions or missile launchings) | 7 | 33 |
| Fractional orbit bombardment system (FOBS) | 18 | 0 |
| Ocean surveillance | 12 | 0 |
| Inspector targets | 9 | 0 |
| Inspector destructors (hunter-killer anti-satellite satellites | 7 | 0 |
| Orbital launching platforms | 135 | 0 |
| TOTAL | 826 | 374 |

(Includes 48 DOD civilian payloads)

Source: Staff Report, Committee on Aeronautical and Spcae Sciences, United States Senate, by Charles S. Sheldon II, CRS Library of Congress.

*Both the National Security Council and the Pentagon note there is a mistake in this table, but they are unable to supply clarification.

Reference: J. C. Glenn and G. S. Robinson, Space Trek, The Endless Migration, Stackpole Books, Harrisburg, PA, 1978.

candidate at the low-power levels because of survivability considerations. At the higher-power levels, reactors become the prime candidate because of cost and survivability considerations. For space defense, large quantities of power may be needed for short periods of time (less than an hour). This could mean chemical power or electrical power with some type of storage device. Another large power need is for orbital transfer and maneuvering. Ion propulsion using electrical power in the hundred kilowatt range offers many advantages for this.

Within the Space Command context, we can examine specific elements for their power requirements. It should be remembered that all of these elements will be necessary for an integrated effective operational force -- surveillance for detection, communications for command and control, weapons to resist attackers and to destroy enemy targets, and a command center to provide the human decision-making element and tactical implementation. In some areas, nuclear electric power plants become an enabling technology while in others it offers definite benefit/cost advantages. The current nuclear electric power plant named SPAR is aimed at providing 100 $kW_e$.

To define the conditions where SPAR is an enabling technology, we used the following criteria. An operational military satellite should require no more than two Space Shuttle trips. Because the three-stage chemical Inertial Upper Stage (IUS) can deliver about 3000 kg to geosynchronous orbit, this limits the total satellite weight to about 6000 kg. However, SPAR with electric propulsion can place a 10,000 kg payload in geosynchronous orbit or for two Space Shuttle trips, the limit is 20,000 kg. This means that a single SPAR power plant with electric propulsion can do what a chemical system does in three or four Shuttle trips. The other enabling criteria is the power level for high-orbital satellites. Above about 25 $kW_e$, advanced solar arrays with batteries require too much of the Space Shuttle bay capacity (more than the traditional 30% weight for the power supply).

Among the missions that nuclear power may be considered enabling based on these criteria are:

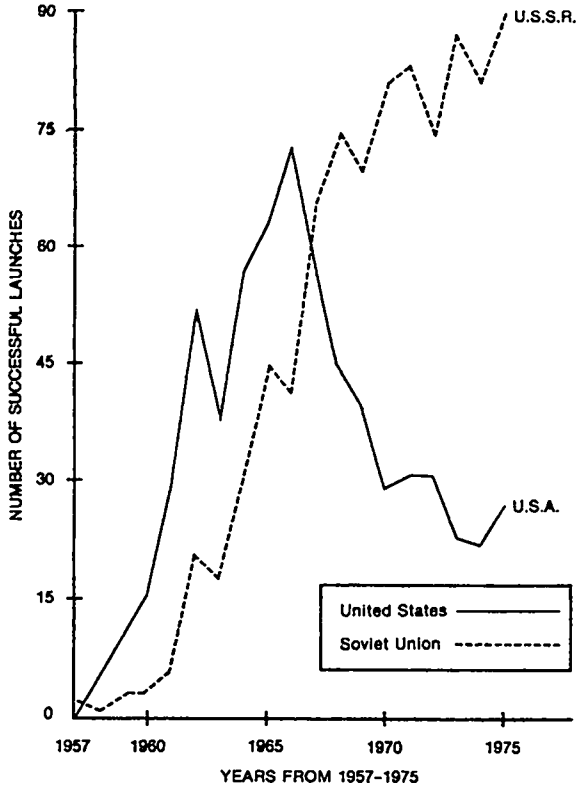


Source: Staff Report, Committee on Aeronautical and Space Sciences, United States Senate, by Charles S. Sheldon II, CRS, Library of Congress

Chart by Future Options Room Washington, D.C.

| SUCCESSFUL LAUNCHES | U.S. | U.S.S.R. |
|---|---|---|
| Civil | 323 | 292 |
| Military | 326 | 586 |

Reference: J. C. Glenn and G. S. Robinson, Space Trek, The Endless Migration, Stackpole Books, Harrisburg, PA, 1978.

Fig. 2. U.S.-Soviet record of known successful space launchings.

- Multimission space-based radar to track missiles, aircraft, and satellites;
- Multimission infrared trackers for missiles, aircraft, and satellites;
- Deep-space command center for secure and survivable command post for strategic forces;
- Tactical and strategic communications with high anti-jam capability for use with mobile terminals;
- Real-time battle communications for use by troops in the field;
- Navigation grid projection to identify locations within a battlefield;
- Control of Remote Piloted Vehicles from remote locations;
- Anti-satellite and satellite defense for maneuvering and as a possible power source for defense; and
- Real-time weather display for aircraft in flight everywhere in the world.

Besides being an enabling technology, there are some missions where SPAR offers benefit/cost advantages or other mission advantages such as survivability. These missions may be roughly characterized as high-orbital locations with spacecraft weighing between 3000-6000 kg and/or requiring 10-25 $kW_e$ of power. These criteria were selected because they could result in the use of a single Shuttle per satellite with its resultant major reduction in transportation and assembly in space cost. Examples of these are:

- Ocean surveillance radar for tracking ships at sea; and
- Global logistics information center for world-wide inventory control.

B. Potential Peace Keeping and Arms Control Applications

One of the dominant issues in arms control agreements such as SALT is that of verification. On-site inspection has generally been deemed unacceptable. Foreign countries have proven to be uncertain locations of verification sensors such as radar, as witness Iran. Also, foreign bases have limited capability to observe certain areas within the USSR. The solution has been to locate the necessary monitoring sensors in space. However, vastly improved sensors than the current generation will be required if arms control agreements are to be more specific and applied to a greater range of armaments. For instance, if we wish to track force concentrations in a given area, vastly improved radar and optical systems are needed. These may be even larger than the multimission radars contemplated for defense purposes. The technology for such systems appears feasible and would be well worth the cost if they increase the probability of peace and security with reduced armaments. These sensors will require significant amounts of power both for propulsion to geosynchronous orbit and for operation when on station.

The use of satellites for peace keeping has already been demonstrated by the USSR to verify that the Egyptians and Israelis were adhering to the

cease fire in 1973. This type of monitoring appears to be a continuing requirement. Again, large systems in high orbits appear to offer this capability on a global basis.

C. Potential Civilian Earth-Orbit Missions

The U.S. is just beginning to exploit space, yet even these embryonic starts have greatly improved global communications, resource mapping, meteorology, and navigation. On the nightly television news, we take for granted the radar pictures from space of weather patterns and cloud cover sweeping across the U.S. Some of us remember sitting by the radio hearing the clicking of telegraph keys as we heard the World Series. Now, we watch events happening on the other side of the world as they occur, such as the Olympics. This is just the beginning. We can catch up to Dick Tracy with his wrist radio communication device. New manufacturing capabilities will exist where higher performance materials, such as magnets, ultrapure glass, and silicon are possible products.

The number of potential missions is long. Following is a list that was selected based on their potential weight, power requirements, and location in geosynchronous orbit. The work of I. Bekey, A. I. Mayer, and M. G. Wolfe[2] was used since it categorized a number of these applications by function, weight, size, power, orbit, time frame, initial operating cost, and risk. These missions include:

- Personal communications wrist telephones to serve 2.5 million people.
- Police wrist radio communications to provide real-time, secure, anti-jam, high-coverage, wide-area personal communications for policemen.
- Disaster communications to provide command and control for area emergency personnel.
- Electronic mail to transmit facsimiles of letters at reduced cost.
- National information services to provide small users rapid access to information.
- Voting or polling wrist set to provide convenient, rapid determination of the electorate's stand on candidates and issues.
- Advanced television antenna systems to provide improved television coverage, especially to mountainous, rural, and remote areas.
- Border surveillance to detect illegal aliens, drug traffickers, and others who are attempting overt or covert crossings of the border using small, sensitive, seismic sensors planted along the border and monitored from space.
- Energy monitor to fine tune energy distribution by monitoring current, voltage, or power readings on the network.
- Vehicle and package locators to be used to monitor shipments throughout the U.S. continuously and thereby minimize thefts, hijackings, and lost shipments.
- Three-dimensional holographic teleconferencing to reduce the need for travel and thereby save considerable time and money. Laser illuminators and stero sound would give the impression that all participants are present and active at the meeting.

Figure 3 shows that the above mission power requirements range from 15-220 $kW_e$ and mass from 3000-9000 kg.

D. Solar System Exploration

Our desire to explore the universe goes beyond doing it just because it is there. An understanding of other planetary bodies leads to a much greater understanding of our own planet. Space exploration has made us realize that earth is a space-ship with limited resources and a delicate environment. With planets closer and more distant from our Sun, we can trace different stages in planetary evolution that provides clues to our own planet's past and future. Planetary exploration also provides us a chance to better understand the natural laws that govern all processes. Using the Earth as a vantage point for understanding the behavior of nature is limited by forces such as gravity and magnetisms that are associated with Earth's environment. As we reach out into space, we are able to observe phenomena not discernible within the Earth's environment that may lead to fundamental changes in our definition of the laws of physics. This better understanding might someday lead to solving everyday problems such as fusion for unlimited energy. Besides an improved knowledge of the solar system and improved understanding of scientific phenomena, planetary exploration is laying the foundation for future exploitation of space resources and possible colonization. Also, we are taking our first small steps to other stars.

Solar system exploration missions are being performed at greater distances from the earth and in

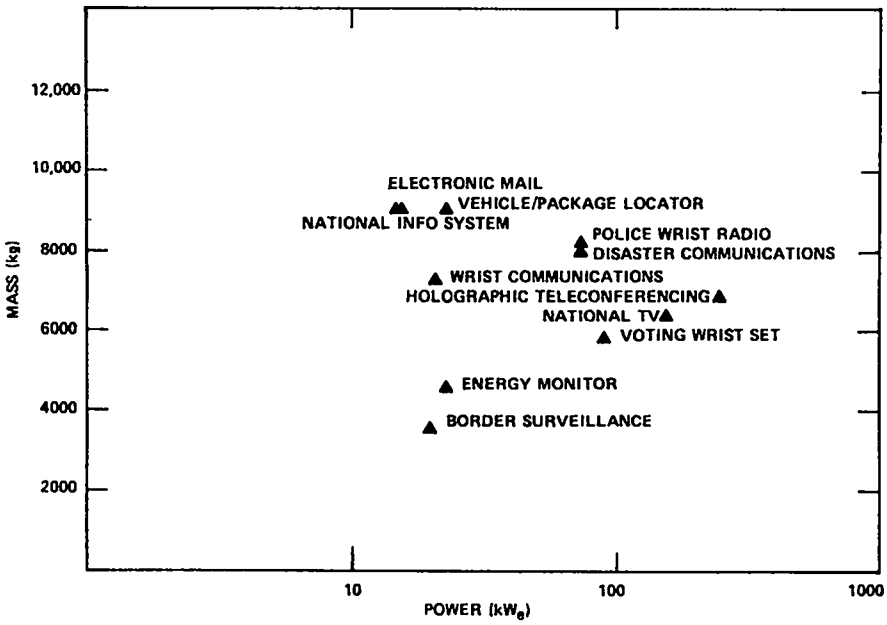


Fig. 3. Potential civilian applications in geosynchronous orbit.

ever increasing detail. Exploration has progressed from reconnaissance probes of bodies in the solar system to the exploration of these bodies with orbiting sensors and landers followed by intensive studies using rovers and surface sample and return techniques, and may finally lead to establishing semipermanent or permanent bases.

Figure 4 depicts expected growth for planetary missions with the capability expected from various propulsion modes.[3] Chemical power has been the major propulsion source to date, but the limits of its capability will be reached in missions during the 1980s. Solar Electric Propulsion (SEP) with ion thrusters will extend the ability to perform planetary missions and meet requirements for the late 1980s and early 1990s, but its limit will be reach in reconnaissance missions to Uranus and exploration missions to Saturn. Nuclear Electric Propulsion (NEP) with ion thrusters extends the capability to investigate the outer planets and to perform solar escape missions. The nuclear electric propulsion power supply envisioned here uses a 400-$kW_e$ power plant. A significant advantage is obvious for nuclear electric propulsion, especially as the distance from the Sun increases.

A 100-$kW_e$ power plant such as SPAR can provide significant capability over the SEP system shown in Fig. 4, and provide the experience and technology base for the longer duration, more distant missions to Pluto and beyond. For instance, based on recent studies at the Jet Propulsion Laboratory, the payload to the Asteroids is tripled using SPAR as a power source for electric propulsion and reconnaissance missions to Uranus and Neptune become feasible. Nuclear power is an enabling technology if we are to pursue our planetary program to the outer planets.

E. Transportation to Geosychronous Orbit

A number of candidate systems exist to move satellites from low to geosynchronous orbit. Some of these are one-time-only systems and others are based on reusable vehicles. The characteristics of the transfer will determine the type of propulsion desirable. Chemical systems tend to perform the transfer in a matter of hours at high acceleration levels. Electrical propulsion with ion thrusters take hundreds of days to perform a similar transfer. However, the stage weights are considerably less with ion thrusters. Chemical rockets can be characterized as high thrust but limited specific

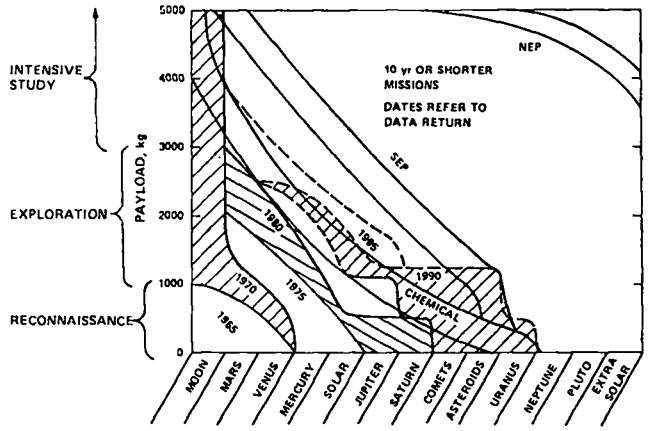


Fig. 4. Solar system exploration.

impulse systems, while electrical propulsion are limited thrust but high specific impulse systems. A number of potential orbital transfer vehicles are compared in Fig. 5.

The Inertial Upper Stage (IUS) that is currently being developed as a standard module for the STS consists of a two-stage vehicle 4.5 m in length. It is capable of transporting a payload of 2270 kg to geosynchronous orbit. There is also a three-stage version that is formed by adding another large motor as a lower stage to the two-stage vehicle. It is 6.4 m in length and can deliver 3180 kg to geosynchronous orbit.

Transtage, Agena, and Centaur, current upper stage chemical rockets, provide limited payloads to geosynchronous orbit. A number of advanced chemical stages, Low Thrust Liquid (LTL), All Propulsion Orbit Transfer Vehicle (APOTV), and Aeromaneuvering Orbit Transfer Vehicle (AMOTV) are being investigated. The LTL can deliver twice the payload to geosynchronous orbit as a three-stage IUS. Also shown in Fig. 5 is the nuclear electric propulsion stage (NEPS) using a 100-$kW_e$ power plant. The delivery capacity is three times that of the three-stage IUS. NEPS can deliver large payloads compared to chemical stages, but at a cost in delivery time (150-225 days compared to one day or less).

If solar arrays are incorporated into the spacecraft, then these can be used as a power source for ion thrusters. Because of higher mass and large volume, solar arrays can deliver about half the mass and require twice the time compared to nuclear electric propulsion. One reason for their poorer performance is that about one-third of the solar array power is lost from degradation in the Van Allen belts.

Nuclear power appears to offer an interesting option for one-way transfer of spacecraft to geosynchronous orbit or possibly as a space tug (depending on safety aspects) where transfer times of a half year are acceptable. The larger payload capability compared to either chemical stages or solar arrays and the ability to endure long time periods in the Van Allen belts are definite advantages. In addition, experience will be gained for planetary missions in the 1990s.

F. Power Plant Requirements

1. POWER OUTPUT. Nuclear power requirements in geosynchronous orbit cover the range from 10-100 $kW_e$ for potential defense missions and 15-220 $kW_e$ for potential civilian applications. For planetary missions, 400 $kW_e$ appears desirable.

2. LIFETIMES. Lifetimes are established by anticipated development of other components in the spacecraft. Goals of 7-10 years have been established for spacecraft in geosynchronous orbit and 10 years for planetary missions.

3. RELIABILITY. Power subassembly reliability of 0.95 is the design goal for geosynchronous orbit and as high as possible for planetary missions. Designs that avoid single-point failures and degrade gradually are favored.

4. MASS. A general rule of thumb is that the power subassembly will require up to 30% of total space mass. For a dual Shuttle-launch spacecraft, the goal is 1910 kg.

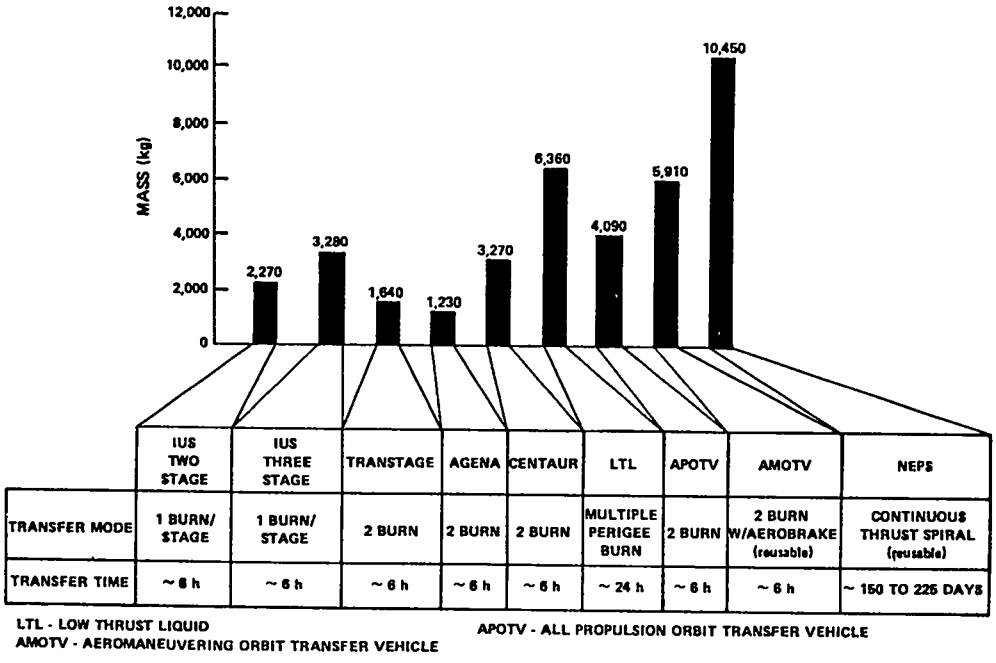


Fig. 5. Orbit transfer system performance comparison (low earth orbit to geosynchronous orbit).

5. CONFIGURATION CONSTRAINTS. The Space Shuttle dimensions of 18.3 m length and 4.5 m diameter limit the volume allowable for the power source. The individual spacecraft will determine how much volume can actually be used by the power source.

6. RADIATION. The spacecraft must be able to operate in natural radiation fields. Induced radiation created by nuclear power systems must be reduced to an acceptable radiation level determined by spacecraft components. For present electronic components, it is $10^{13}$ nvt and $10^{7}$ rad over the mission life.

7. SAFETY FEATURES. The power subassembly must meet all regulations of NASA, DoD, DOE, and the National Range Commanders. All payloads using the STS are subject to a uniform set of basic safety and interface verification requirements. The safety requirements are tailored to identify the hazard potential of the payload. The Payload Safety Guidelines Handbook (JSC-11123) provides a basis for selecting design options to eliminate hazards. The STS safety policy requires that the basic payload design assure the elimination or control of any hazard to the Orbiter, crew, or other payloads.

Table II provides a summary of power plant requirements.

## II. POWER PLANT DESCRIPTION[4]

### A. General Configuration

An extensive review of design alternatives for a nuclear reactor space power system capable of delivering 10-100 $kW_e$ has led to the selection of a heat-pipe-cooled fast spectrum reactor with a thermoelectric power conversion system. The general features of this system are illustrated in Fig. 6. The reactor design features a beryllium reflector, laminated core configuration with sheets of molybdenum extending across the full diameter of the core and interspersed between layers of $UO_2$. Reactor heat is transferred by the sheets from the $UO_2$ to an array of some 90 Mo/Na heat pipes. The heat is then transported by the heat pipes around the LiH shield to a ring of high-power density thermoelectric modules constructed from modified SiGe alloys. Conversion takes place over a temperature interval of 1375-775 K with an efficiency of 9%. Residual heat is rejected by a radiator that is constructed using heat pipes.

Avoidance of single point failures and propagating failure chains has constituted the main design emphasis for the SPAR system. Currently, no single failure points are known to exist in the power

TABLE II

POWER PLANT REQUIREMENTS

| | Requirement | |
|---|---|---|
| | Geosynchronous | Planetary |
| Power output ($kW_e$) | 10-100* | 400 |
| Lifetimes (y) | 7 | 10 |
| Reliability | 0.95 | High as possible; no single point failures |
| Mass (kg) | 1910 | 8000 (includes power conditioning and larger shield) |
| Configuration constraints | Minimize packaging volume in shuttle bay | Minimize packaging volume in shuttle bay |
| Radiation attenuation | | |
| Neutrons (nvt) | $10^{13}$ | $10^{12}$ |
| Gamma (rad) | $10^{7}$ | $10^{6}$ |
| Maneuverability | Mission dependent | Ion thrusters |
| Safety | STS requirements | STS requirements |

*NASA requirements could extend this to 220 $kW_e$.

plant. Thus, the core contains 90 separate thermally-coupled heat transfer loops, each with an associated power conversion module. Connecting modules in a series-parallel network makes it possible to tolerate the loss of several of these units while still maintaining operational capability for the system as a whole. Interconnecting the heat pipes in the waste heat removal system yields a network that is highly tolerant of heat pipe failures.

B. Reactor Design and Shield

Early designs of the SPAR core featured hexagonal fuel elements of molybdenum-encased UC-ZrC, each of which was cooled by a separate heat pipe constructed of molybdenum with sodium working fluid. Interelement heat transfer, required to accommodate potential core heat pipe failures, was to be achieved by a core banding system that established thermal contact by compressing deformable foil placed between fuel elements. This system had a number of design uncertainties that would have required extensive development and testing to resolve. It was also difficult to power flatten, partly due to its basic hexagonal geometry. However, it was not these considerations but rather the desire to avoid the development and fabrication problems anticipated for the carbide fuel that set in motion the innovation chain leading to the present design. Specifically, it was the desire to build a $UO_2$-fueled core without sustaining too large a reactor size and weight penalty that led to a layered Mo-$UO_2$ fuel configuration that was eventually expanded from a single fuel element to the current integral core design.

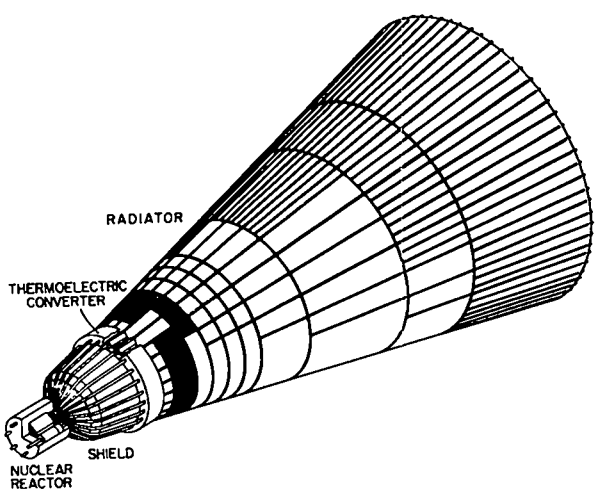


Fig. 6. Layout of SPAR power plant.

The integral core SPAR design is shown in Fig. 7. The core is contained within a cylindrical molybdenum can having a diameter of 290 mm and a height of 290 mm. Because the can is not designed as a pressure vessel, its walls and one end plate are only 2 mm thick. The other end plate, which serves as the mounting plane for the heat pipes, is 6 mm thick. Within this can are 90 molybdenum heat pipes encased in a fuel that consists of alternate layers of $UO_2$ and molybdenum. The core is reflected radially and on one end by beryllium. The other end reflector is BeO that is mounted around the heat pipes within the molybdenum core container. Control of the reactor is provided by twelve rotating beryllium drums each with $B_4C$ segments mounted on one side. Key design parameters of the reactor are given in Table III.

The interleaving of sheets of molybdenum between layers of $UO_2$ has provided a fuel form that has

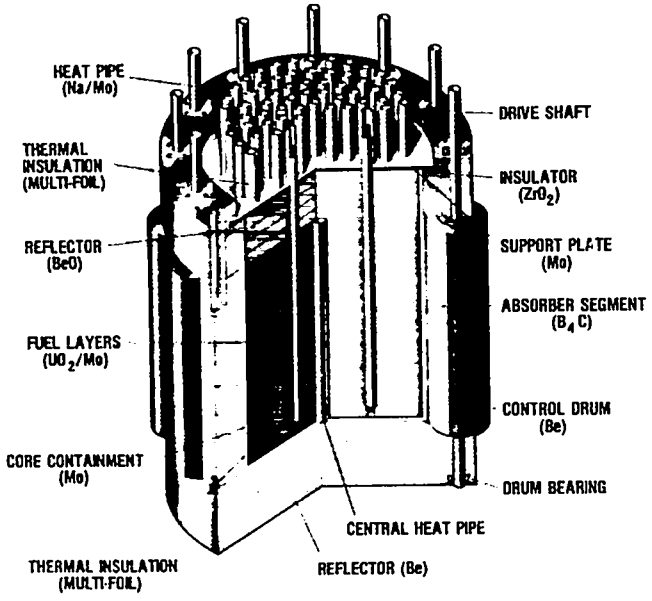


Fig. 7. Cutaway view of SPAR assembly.

made possible a relatively compact $UO_2$-fueled core with a number of design simplifications over previous SPAR configurations. Compactness results from the high volume fraction of $UO_2$ in the fuel. This could be done without causing excessive fuel temperatures because the layered configuration maximizes the thermal conductivity of the fuel for a given amount of added molybdenum.

Figure 8 shows one method by which the layered fuel can be attached to heat pipes. Heat generated in the $UO_2$ is conducted to the molybdenum sheets and thence along these sheets to the heat pipes,

TABLE III

SPAR DESIGN PARAMETERS

| | | |
|---|---|---|
| Reactor Power ($kW_t$) | | 1100 |
| Core diameter (mm) | | 290 |
| Core height (mm) | | 290 |
| Number of core heat pipes | | 90 |
| Core heat pipe temperature (K) | | 1400 |
| Reactor diameter (mm) | | 520 |
| Reactor height (mm) | | 500 |
| Reactor mass (kg) | | 400 |
| Fuel region | 125 | |
| Reflector | 160 | |
| Heat pipes | 55 | |
| Control system | 35 | |
| Support structure | 25 | |

where thermal contact is made by a spring tab configuration. Each sheet is in thermal contact with the entire complement of core heat pipes. The core is built up by pressing one sheet at a time over the heat pipe array, which is held firmly in place by the molybdenum end plate. The $UO_2$ is in the form of tiles, shaped as shown in Fig. 8. A complete layer of these tiles can be attached to each molybdenum sheet with a vaporizable bonding agent to simplify assembly.

One of the important design simplifications that has been made possible by the layered fuel configuration is that the core is cylindrical. This not only reduces critical mass because of reduced neutron leakage, but also eases the assembly procedure and makes the reflector design more tractable. The layered fuel adds confidence to the ability of the system to withstand heat pipe failures because it removes the concern with thermal bonding between fuel elements. It markedly improves the tolerance of the system to failure of heat pipes on the core

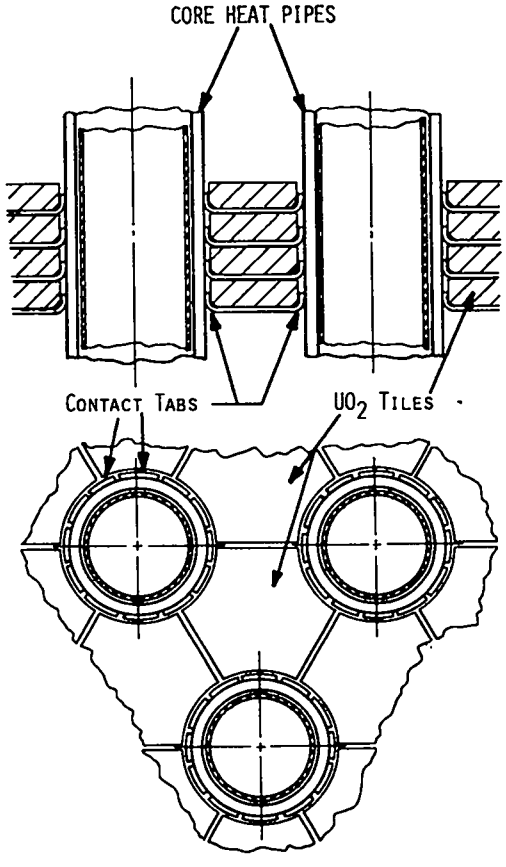


Fig. 8. Layered Mo-$UO_2$ fuel arrangement.

periphery because the outer molybdenum can is able to serve as an additional thermal conduction path for removing heat from the fuel surrounding an inoperable heat pipe and transporting it to neighboring heat pipes.

Perhaps the most important design simplification made feasible by the layered fuel concept is the ease with which radial power flattening can be achieved. This can now be done by arranging the heat pipes in concentric rings and varying the spacing between heat pipes from one ring to the next so that the total heat flux transmitted to each heat pipe is constant. This is accomplished with no variation in fuel enrichment. Hence, no significant increase in core size and mass is needed to produce a power-flattened core.

Still another simplification feature attributable to the layered fuel configuration is the manner in which fuel swelling can be accommodated. Room for radial fuel swelling can be obtained by allowing space between $UO_2$ tiles. Space for axial swelling is easily introduced, where necessary, by periodically leaving unfilled space between the molybdenum sheets when the stack is assembled.

Shield design and technology make extensive use of work on space reactor shields for SNAP 2, 8, and 10A, and of ROVER experience. These reactors have certain features in common with current designs, namely, small physical size, unmanned space application with comparable allowance for neutron and gamma doses, and comparable radiation flux levels.

Only shadow shielding is required because:

- Only unmanned power plant operation is considered.
- The reactor will be used only in high-Earth orbit, where neutron and gamma scattering from air is negligible.
- The reactor can be located at one end of the assembly, followed by the shield, control actuators and radiator, and, finally, the payload.

The shield can be considered as follows: Neutron attenuation is provided by lithium hydride (LiH) in the shape of a frustum, and a heavy-metal gamma shield is added at the reactor end of the shield if needed.

Lithium hydride dissociates unless an overpressure of hydrogen is provided. Also, the LiH is maintained at a minimum temperature of 600 K during operation so radiolytically decomposed hydrogen will be reabsorbed by the LiH and prevent swelling.

To minimize single-point failures, the LiH is to be encapsulated in a number of pancake-shaped cans so that pressure containment failure from meteoroid penetration or a weld failure, for example, will deplete the hydrogen in only a small part of the shield. The shield is also a structural member that connects to the reactor on one end and by a boom to the payload on the other.

C. Conversion System and Radiator

Power conversion for the SPAR system is accomplished by a network of thermoelectric elements based on silicon-germanium alloys. These elements are built into cylindrical modules surrounding the core heat pipes as shown in Fig. 9. In this unit, six n-p couples are positioned circumferentially around the core heat pipe in a series configuration that yields approximately 1 volt output under normal operating conditions. The module is formed by placing these ring units adjacent to each other along the pipe, the number being determined by the output voltage desired. For power levels of 100 $kW_e$, a voltage level of 100-150 Vdc is desirable in order to minimize the power transmission line weights.

Not shown in Fig. 9 is the system to remove reject heat from the outer periphery of the module. This can be done either by a single annular heat pipe enclosing the entire module or by a redundant system of small annular heat pipes about each of the thermoelectric ring units. The latter configuration is illustrated in Fig. 10. The coupling heat pipes

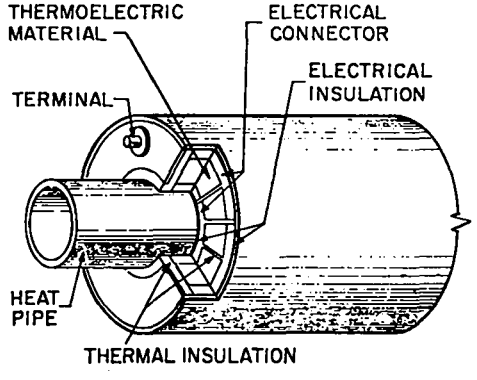


Fig. 9. High power density thermoelectric module.

serve to change the geometry from cylindrical to square in order to achieve good thermal contact with the radiator stringer pipes. The latter are shown with a rectangular cross section at the evaporator end and are arranged so that several cool each thermoelectric module.

As Fig. 10 illustrates, five thermoelectric modules are grouped together to form a basic panel segment of the thermoelectric conversion and radiator subsystems. The coupling heat pipes of adjacent thermoelectric modules are thermally connected so that if one of the radiator stringer heat pipes should fail, its heat load is shared by nearby stringers.

The stringer heat pipes are made of titanium because of its relatively low density combined with high temperature capability. Current designs are stressing minimal heat-pipe wall thickness and the potential use of lightweight armor layers such as carbon, silicon, aluminum, or refractory compounds on the side of the stringer exposed to meteoroid flux.

The manner in which the radiator panels are displayed to form the full radiator is illustrated by Fig. 11. With a total of eighteen segments, the array is approximately cylindrical with a diameter that just fits into the bay of the shuttle launch vehicle. The cylindrical configuration is favored because packaging considerations in the shuttle bay may rival power plant mass in importance. The radiator is a dominant length element and can be packaged in a number of configurations (Fig. 12). The cylindrical arrangement is very convenient because it allows storage inside the radiator during shuttle

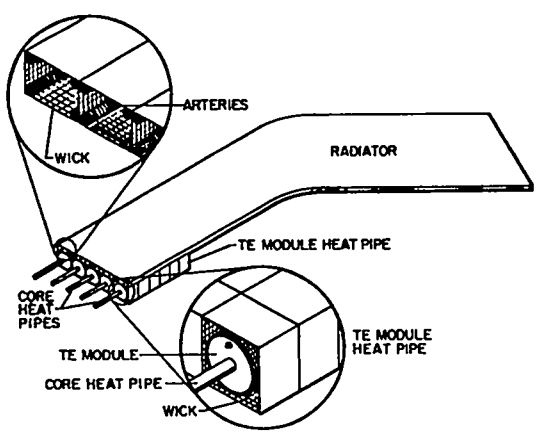


Fig. 10. Radiator segments.

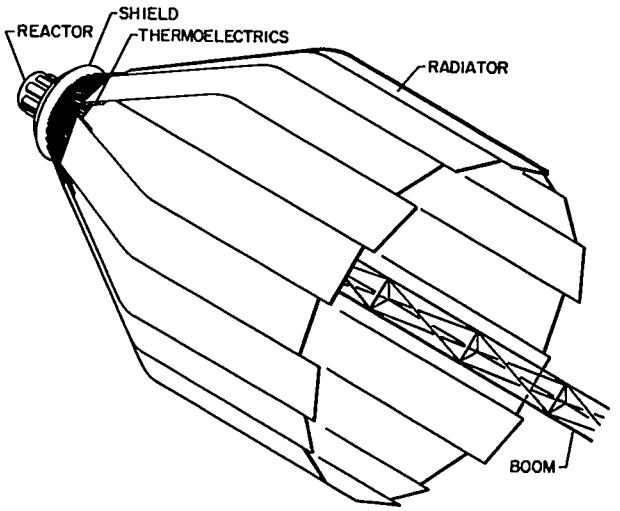


Fig. 11. Space nuclear power plant.

flight. Figure 13 shows a structure stored inside the radiator in stowed and partially deployed configurations.

D. Operating Parameters for 10-100 $kW_e$ Power Plants

Table IV gives operating parameters for the SPAR system at various design powers. The thermoelectric module efficiency is taken to be 9%. This value is based on work done on SiGe alloys modified with GaP additive to decrease thermal conductivity.

E. Power Plant for 400 $kW_e$

Design studies of a nuclear reactor to provide thermal power to an electric propulsion system for deep space exploration have been ongoing for several years. The present design goals are to produce 3 $MW_T$ of power for 75,000 full-power hours during a mission lifetime of 12 years to drive a thermionic electrical conversion system operating at a source temperature of 1650 K.

The reactor design has evolved to a configuration very similar to the one for 1.2 $MW_t$. However, it contains 162 heat pipes. The heat pipes are still molybdenum but, because of the higher temperature, they use lithium as the working fluid. Figure 14 is a layout of the core. The reflector is all BeO because of the higher operating temperature, and the number of control drums is increased to 16 because of the larger core diameter.

The reactor design is described in Tables V-VII. Fuel swelling for the layered integral core design was estimated from BMI data[5] for pure $UO_2$, which

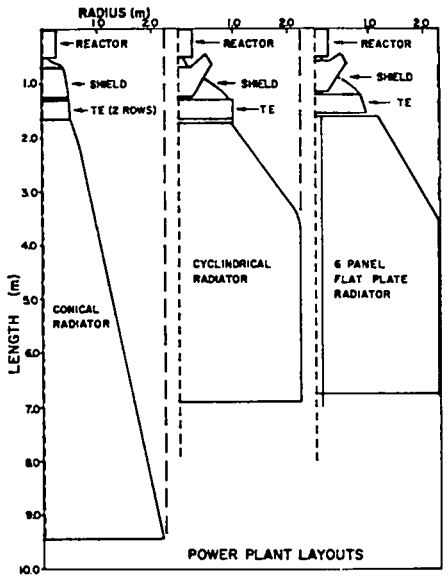


Fig. 12. Power plant layouts.

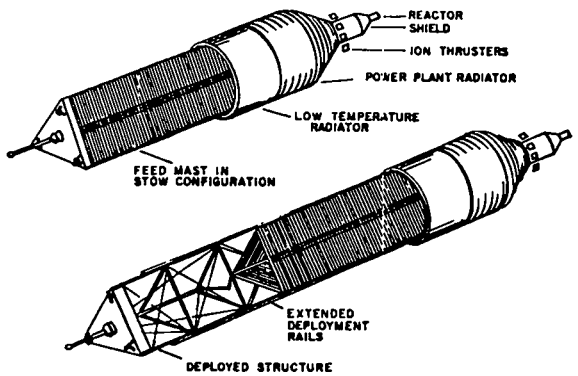


Fig. 13. Nuclear OTV stage.

has a considerably higher swelling rate than $UO_2$ in a molybdenum matrix. It is not clear that the BMI data is directly applicable to the layered core concept because the temperature gradient in the $UO_2$ will be much smaller in the reactor than it was in the BMI experiments. As a consequence, it is possible that swelling extrapolated from this data is overestimated. In any case, the required void allowance for fuel swelling can easily be incorporated in the layered core design simply by including gaps between layers in the core, and between the $UO_2$ tiles.

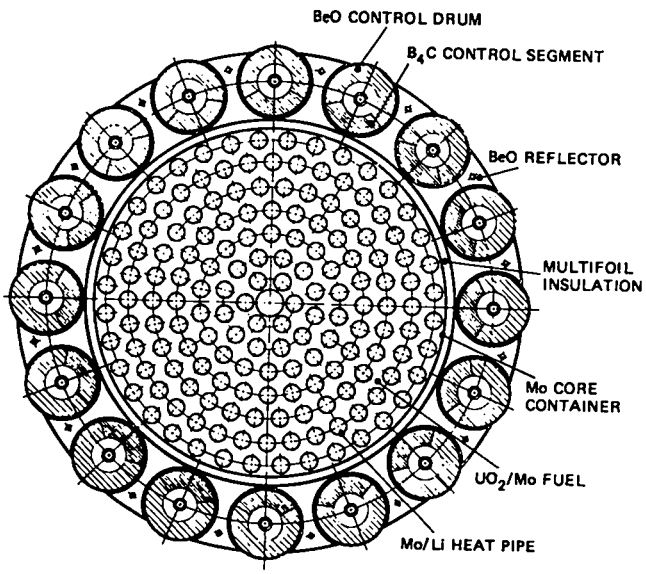


Fig. 14. Cross section of a 3-MW layered integral core reactor.

TABLE IV

OPERATING PARAMETERS OF SPAR THERMOELECTRIC POWER PLANT (7 yr Lifetime)

| | Power ($kW_e$) | | |
|---|---|---|---|
| | 10 | 50 | 100 |
| Reactor power ($kW_e$) | 110 | 550 | 1110 |
| Core heat pipe temperature (K) | 1400 | 1400 | 1400 |
| Fuel swelling (%) | 1 | 2 | 3 |
| Burnup fraction - $^{235}U$ (%) | 1 | 2 | 4 |
| Thermoelectric efficiency (%) | 9 | 9 | 9 |
| Radiator temperature (K) | 775 | 775 | 775 |
| Radiator power ($kW_t$) | 100 | 500 | 1010 |
| Power plant mass (kg) | 810 | 1255 | 1775 |
| Reactor | 400 | 400 | 400 |
| Shield | 255 | 335 | 380 |
| Thermoelectric converter | 30 | 140 | 285 |
| Radiator | 50 | 255 | 530 |
| Structure | 75 | 115 | 160 |

TABLE V

REACTOR DIMENSIONS

| | Laminated Core |
|---|---|
| Core diameter (mm) | 390 |
| Reactor diameter (mm) | 620 |
| Core length (mm) | 390 |
| Reactor length (mm) | 600 |
| Reflector thickness (mm) | 100 |
| Number of heat pipes | 162 |
| Average heat pipe spacing (mm) | 29.1 |
| Heat pipe outer diameter (mm) | 20.0 |
| Heat pipe vapor area ($mm^2$) | 188 |
| Fuel vol. fraction (assuming 100% dense) | 0.461* |

*80 vol% $UO_2$-20 vol% Mo fuel

TABLE VI

REACTOR WEIGHT SUMMARY (kg)

| | | Laminated Core |
|---|---|---|
| Mo-$UO_2$ fuel, total weight | | 231 |
| $UO_2$ only | 187 | |
| $^{235}U$ only | 154 | |
| Mo heat pipes, 110 kg/m (to outer edge of reactor only) | | 54 |
| BeO reflector | | 342 |
| Control system | | 75 |
| Reactor support structure | | 35 |
| TOTAL | | 737 |

TABLE VII

REACTOR OPERATING CHARACTERISTICS

| | Laminated Core |
|---|---|
| Nominal electrical power output ($kW_e$) | 400 |
| Thermal power level ($MW_{th}$) | 3 |
| Thermionic converter efficiency (%) | 15 |
| Lifetime at full power (h) | 75000 |
| Number of heat pipes | 162 |
| Nominal $UO_2$ content of fuel (vol %) | 80 |
| Average power density in Mo-$UO_2$, ($MW/m^3$ or $W/cm^3$) | 114 |
| Average power density in $UO_2$, ($MW/m^3$ or $W/cm^3$) | 143 |
| Power per heat pipe (kW) | 18.8 |
| Heat pipe axial heat flux ($MW/m^2$) | 100 |
| Heat pipe radial heat flux ($MW/m^2$) | 1.00 |
| Heat pipe temperature (K) | 1675 |
| Average fuel temperature (K) | 1763 |
| Maximum fuel $\Delta T$ (K)* | 199 |
| Maximum fuel temperature, (K)* | 1906 |
| $^{235}U$ burn up (%) | 7.1 |
| Fission density in Mo-$UO_2$ ($10^{20}$ fissions/$cm^3$) | 9.2 |
| Fuel volume swelling (%) | 20 |
| Reactivity change $\Delta k$ due to fuel burn up (%) | 4.3 |
| Reactivity change $\Delta k$ due to thermal expansion (%) | 2.1 |

*Assumes a 1.5 peak-to-average power density ratio.

## III. SAFETY ASPECTS OF A NUCLEAR POWER SOURCE

The US position concerning safety of nuclear reactors in space is summarized in the following excerpts from a working paper submitted to the United Nations Committee on the Peaceful Uses of Outer Space, Scientific and Technical Sub-Committee, in February 1979.

> "U.S. safety philosophy relative to space reactors has not been re-examined since the development and launch of the SNAP 10A SNAPSHOT. However, the basic design philosophy developed for that launch is, in principle, still valid." ...The basic safety requirement is no undue risk to the public or the environment. In the case of nuclear reactors which have operated, the primary concerns are the release of fission products from the reactor core and high-level external radiation from an intact core or from activated components of the reactor's structure. These concerns can be minimized or eliminated by restricting the use of the reactor to high earth orbit. Hence, a basic criterion for space reactor operation could be to launch unoperated reactors which are started after a safe altitude is confirmed. The U.S. currently defines a safe altitude as one where the lifetime is greater than 300 years (400 nautical mile circular orbit). This would allow sufficient time for the fission products and activated materials to decay to safe limits before reentry. Another consideration would require controls to prevent inadvertent criticality of the reactor in the event of launch accidents."

The key to safe operation before and during launch is to keep the reactor in a nonoperative mode. This is accomplished by adding built-in safety features, such as redundant control elements, where only one element is allowed to be unlocked at a time; brakes on the control element actuating mechanisms to prevent movement without two independent signals; and a reactor designed to remain nonoperative even with environment changes, such as immersion in water. Before operation, the reactor and its uranium fuel are perfectly safe to handle. There is no possibility that a nuclear explosion can result from a space reactor power plant.

Analyses and tests are used to demonstrate safety aspects in case of launch pad fires, propellant fire, impact at terminal velocity in case of a launch abort or failure to reach orbit, and water impact. Again, the major requirement for safety is not to operate the reactor until the prescribed orbit is reached.

Most applications considered for nuclear reactors are in high orbits, such as geosynchronous. The higher the orbit, the longer a satellite will remain in orbit. Long orbit times provide time for radioactive elements to decay. An orbit altitude of 400-500 n mi will provide for over a 1000-yr life and thus could give a margin of conservatism in meeting safety criteria. Doubling the orbit increases the orbital lifetime to about a million years. Satellites in geosynchronous orbit (19 400 nautical miles), the proposed location of most reactor-powered US satellites, will, for all practical purposes, never re-enter the Earth's atmosphere.

The only US reactor flown in space, SNAP 10A in 1965, was not operated until its 700-n mi orbit was achieved. SNAP 10A's estimated orbital lifetime is 3800 yr.

Current US design philosophy is to have the reactor disintegrate and the core disperse on reentry into the atmosphere. This can be accomplished by atmospheric heating, chemical reactions with the atmosphere, and physical forces imposed by the reentry into the atmosphere. The reflector could act as a heat shield on re-entry and, hence, it will be necessary to design it to separate in the upper atmosphere. Though the details of space nuclear power system designs are under development, we anticipate that the reflector will be held together by bands that will melt on reentry as a result of atmospheric heating. The molybdenum heat pipes and structure in the core will oxidize, allowing the fuel to disperse into the atmosphere. The radiation level of any element or particles reaching the Earth's surface will be extremely low after the long orbital times provided for radioactivity decay and will not pose a health hazard.

Since nuclear safety is based on the principle of in-depth defense against possible miscalculations, an anlysis has been performed on the effect of the reactor re-entering intact after low-altitude orbit operation followed by a failure of the nuclear electric propulsion stage. This should be the most serious health hazard to the general population. Even under these circumstances, the radiation levels can still be low enough to not present a health hazard. Figure 15 shows gamma activity as a function of run time for an intact reactor. This information

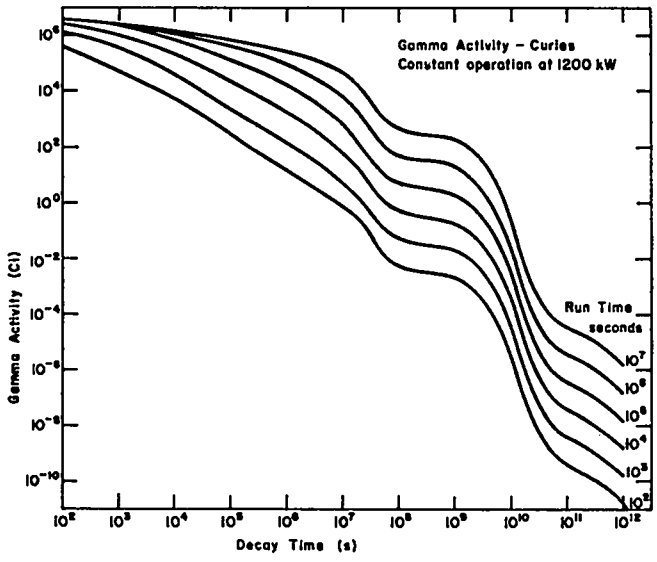


Fig. 15. Gamma activity as a function of time.

was combined with orbital lifetimes before re-entry for different initial starting altitudes and for different power plant operating times prior to a terminating operation. The initial orbits were based on the number of Orbital Maneuvering Subsystems (OMS) employed with the STS. Figure 16 is constructed on the assumption that the reactor will be operated the equivalent of one-hour full power prior to activation of the ion thrusters to checkout the power system. Then, the altitude was computed for 1 hr, 1 day, 1 week, and 1 month of operation and an orbital lifetime determined assuming a spacecraft failure at these points in time. Using Fig. 15, the gamma activity was determined at the time of re-entry and this information is plotted in Fig. 16. The safety region in Fig. 16 represents approximately a 300 yr orbit time. The following conclusions, based on the assumption that somehow the power plant would reach the Earth's surface intact, are reached after examining the figure.

- If two OMS kits are used so that the initial orbit is 850 km (460 n mi), regardless of the time that a failure occurs after initiating reactor operation, there would be no risk to the general population;
- If one OMS kit is used so that the initial orbit is 620 km (335 n mi), the possible risk period is a few days;
- If no OMS kits are used starting at an altitude of 450 km (240 n mi), the possible risk period is about a week.

It is concluded that orbital transfer with a nuclear space power system can be made very safe from a low orbit and as higher altitudes are achieved by the nuclear propulsion transfer vehicle, the system becomes increasingly safe.

## IV. PROGRAM PLAN FOR 10-100 $kW_e$ POWER PLANT

A technology readiness program has been initiated to demonstrate that key components of the reactor/thermoelectric power system can be constructed to meet performance objectives for the required 7-10 yr lifetime. The goal of this program is to bring the power plant technology to the point where the technical risk involved in undertaking the building and testing of a groundbased prototype of the system is low. The general types of information needed to reduce this risk include: understanding the basic physics; knowledge of basic material properties; demonstration of our ability to fabricate the components of the power plant; demonstration that these components will behave as specified; understanding of power plant assembly; and demonstration of our ability to meet safety requirements.

The basic physics of the power plant and its components is straightforward for today's

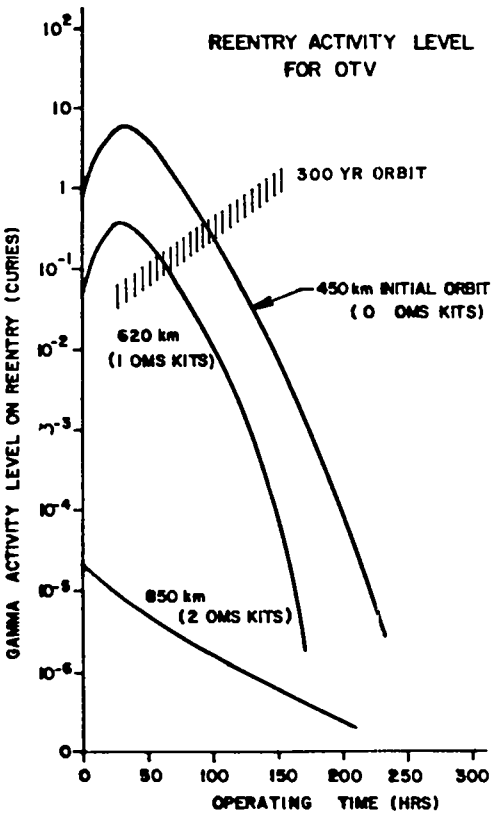


Fig. 16. Reentry activity level for OTV.

technology. Reactor neutronic and kinetic calculations, radiation shielding, converter technology, and radiator technology are all well established. The state of understanding of the properties of the materials used in the SPAR system is not quite so complete. In general, sufficient data exists to give high confidence in the technical feasibility of the SPAR design, but in some instances extrapolation of known data to the 7-10 yr lifetime of SPAR engenders uncertainties that have been compensated by increasing system weight.

Some of the design innovations of the SPAR system call for fabrication procedures that have not been specifically applied to the SPAR components. A major part of the technology readiness program is to adapt these procedures to SPAR component production and show, through accelerated testing in simulated launch and space environments, that the resulting components meet the reliability and lifetime requirements. An extension of this activity is the assembly of portions of the power plant to ensure that interactions between sections of the complete thermal and electrical systems are well understood. Such tests will serve to verify the conclusion of the extensive system design and analysis effort that provides the guideline for the technology readiness program.

Overlying the system design and analysis effort and technology readiness program is the consideration of system safety. The determination of what constitutes safe launch procedures and safe operation in orbit is not static and modification in reactor design as well as tests in addition to the currently planned water immersion criticality measurements and propellent fire effects must be expected.

The technology readiness program has been indexed in terms of the following system components:

1. Nuclear reactor plus heat pipe system for transferring heat to converter.
2. Radiation shield for protection of payload components from neutron and gamma radiation.
3. Thermoelectric conversion system.
4. Radiator heat rejection system.

The program for developing the reactor technology includes comprehensive engineering design and analysis of the core, reflector and control system with heavy emphasis on the ability to withstand the launch environment, and on safety.

A series of critical assemblies will be constructed, primarily to establish firm data for reactor control and safety analysis. Performance confirmation and reliability testing will be done for the molybdenum core heat pipes and for the fuel/heat pipe combination. The latter testing will include irradiation testing in the EBR-II reactor.

Mechanical actuators for SNAP have been individually tested for over three years. However, the effect of going from three year to seven year periods on the durability of mechanical devices is hard to project. A thorough examination of previous actuator performance data and accelerated testing of actuators will be used to verify technical readiness.

Shield design will rely heavily on Monte Carlo analysis and on work done as part of the nuclear rocket and SNAP space reactor programs. The planned canning of the LiH shielding material in a large number of separate stainless steel containers provides the redundancy needed to offset potential consequences of the appreciable hydrogen overpressure

of this material at temperature on the order of 700-800 K.

The thermoelectric conversion units are based on SiGe alloys because of the high temperature capability and outstanding performance record of this material. The unmodified alloy has only a moderately favorable figure of merit. However, work that has been done on the effect of adding GaP to decrease thermal conductivity and thereby increase the figure of merit has shown great promise that the goal of 9% modular efficiency for the SiGe-GaP modules appears attainable. The module development program is directed towards obtaining the highest possible figures of merit from the SiGe-GaP system, minimizing parameter losses occurring in module construction and demonstrating long-term constancy of output under high-power-density operation.

The radiator design features potassium heat pipes that are longer (5 to 6 m) than any that have been tested. Hence, the development program includes performance verification testing of these pipes as well as long-term reliability testing. A number of fabrication alternatives are available and work will be done to select the most suitable of these. Alternative methods of armoring the radiator heat pipes are being investigated in a subprogram that includes experimental determination of the resistance of lightweight armor materials to hypervelocity impact.

The prime candidate for fuel is $UO_2$-20 vol% Mo. $UO_2$ has been used extensively in other reactors. The major new development is in the core configuration. The probability of successfully designing the core with this fuel is considered high.

Core heat pipe development depends on learning to bend high-temperature heat pipes without loss of wick attachment and manufacturing fine mesh molybdenum screen material. Straight molybdenum heat pipes have a good history of operating at the temperatures of interest. The degree of bending required depends on whether the core heat pipes are routed to the thermoelectric converters through the shield or around the shield. Arterial wick configurations, despite increased fabrication complexity, have significant operational advantages that make them the design of choice.

Developing confidence that components will meet the lifetime of interest presents a major challenge. Accelerated component demonstration testing will be performed on the reactor heat pipes, thermoelectrics, and radiator heat pipes. During the development phase, accelerated testing relationships must be found to verify this approach.

Similar relationships will be sought for irradiation tests of fuel segments that will measure the interactions between the fuel and heat pipes in a simulated power plant environment. The effects of radiation and fission product formation on core heat pipe structure and operation need to be determined. These effects are expected to be small, but experimental verification is needed to develop the confidence to proceed to a demonstration power plant.

Overall, we believe that the risks involved in the nuclear power plant are reasonable and that a high degree of confidence exists in demonstrating technical feasibility. Sufficient experimental data should be available by the end of FY-1983 to proceed to a ground demonstration power plant if potential mission requirements warrant. The activities in the present program will result in a relatively modest investment before commitment to the full-scale ground demonstration of a 10-100-$kW_e$ nuclear power plant.

Currently, the component technology program is funded by the DOE at $2 million per year. This level of funding started in FY-79 and is expected to continue for 5 years. Figure 17 is the program plan for the technical feasibility phase now on-going. Depending on mission requirements, the next phase would be to build a ground demonstration of the power plant. The funding for this would be on the order of $15-20M per year.

## V. EARLY KEY RESULTS

### A. $UO_2$/Molybdenum Thermal Coupling Analysis

In the layered fuel configuration, reliance is placed on the molybdenum sheets to carry heat from the $UO_2$ to the heat pipes. Temperature distributions in this fuel are relatively easy to calculate by assuming that the only heat-flow component in the $UO_2$ is perpendicular to the molybdenum sheets and that the flow path in the molybdenum sheets is radially inward to the heat pipe. This type of analysis has indicated that a four to one ratio of $UO_2$ to molybdenum would give maximum molybdenum sheet temperatures on the order of 200 K above the heat pipe

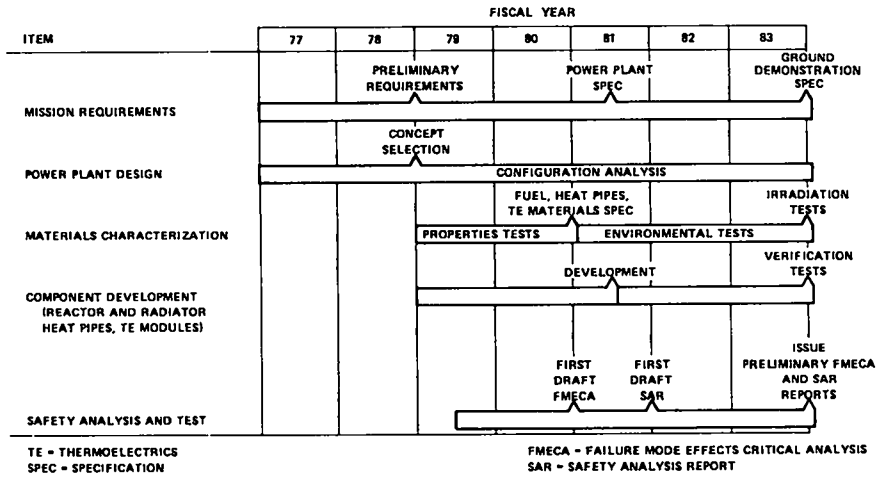


Fig. 17. Program plan.

temperature for an input power density of 116 $MW/m^3$ in the $UO_2$. The maximum temperature in the $UO_2$ tiles depends on the $UO_2$ thickness, with the temperature rise to midplane varying from 20 K for a 2-mm tile thickness to 200 K for 6-mm thickness.

The results of this analysis have been confirmed by a more detailed finite element analysis of the molybdenum sheet/$UO_2$ tile configuration. In this treatment, the thermal contact between the $UO_2$ tiles and adjacent molybdenum sheets was assumed to be either perfect conductive contact or by radiation only, in which case both surfaces were assumed to have the nominal $UO_2$ emissivity of 0.8. In addition, the thermal contact of the molybdenum sheets with the heat pipe was varied from 12.5 to 100% of perfect thermal bonding. Table VIII gives calculated temperatures for the case where the inner heat pipe diameter is at a temperature of 1400 K, the power density in the $UO_2$ is 86.7 $MW/m^3$ (corresponding to a heat pipe location in the core periphery), and the $UO_2$ tiles and molybdenum sheets are 1.6 and 0.4 mm thick respectively.

The table indicates that fuel temperatures are not excessive even when the only transfer of heat from the $UO_2$ to the molybdenum is by radiation and poor contact exists between the molybdenum sheets and heat pipes. The assumption that the molybdenum sheets have the high emissivity of $UO_2$ is warranted by the rapidity with which $UO_2$ will coat the molybdenum because of its non-negligible vapor pressure. Table IX lists $UO_2$ coating times as a function of temperature under the assumption that reevaporation is negligible.

The results in Table IX indicate that establishing good thermal contact between the $UO_2$ tiles and molybdenum sheets in the layered fuel concept is not a problem because high $UO_2$ temperatures that occur because of poor contact are self-corrective - rapidly so in terms of establishing a sufficiently thick $UO_2$ coating (roughly 1 μm) on the molybdenum to produce a high emissivity surface. On a longer-term basis the effective thermal contact will be further improved by the deposition of macroscopically-thick $UO_2$ layers on the molybdenum sheets. Very poor thermal contact between the molybdenum sheets

TABLE VIII

TEMPERATURE OF LAYERED FUEL CONFIGURATION (K)

| Mo sheet/heat pipe contact | Full | 50% | 25% | 12.5% |
|---|---|---|---|---|
| Max. heat pipe temp. exterior wall | 1432 | 1432 | 1434 | 1434 |
| Max. Mo sheet temp. | 1671 | 1689 | 1723 | 1773 |
| Max. $UO_2$ interior temp.: | | | | |
| Radiative transfer | 1861 | 1875 | 1901 | 1941 |
| Conductive contact | 1708 | 1725 | 1759 | 1809 |

TABLE IX

$UO_2$ TRANSPORT

| Temperature (K) | Vapor Pressure[6] (Pa) | Transport Times (s/μm) | (h/mm) |
|---|---|---|---|
| 1400 | $4.0 \times 10^{-9}$ | $1.4 \times 10^{9}$ | $3.9 \times 10^{8}$ |
| 1600 | $1.5 \times 10^{-6}$ | $3.9 \times 10^{6}$ | $1.1 \times 10^{6}$ |
| 1700 | $2.0 \times 10^{-5}$ | $3.1 \times 10^{5}$ | $8.5 \times 10^{4}$ |
| 1800 | $2.0 \times 10^{-4}$ | $3.2 \times 10^{4}$ | $8.9 \times 10^{3}$ |
| 1900 | $1.6 \times 10^{-3}$ | $4.1 \times 10^{3}$ | $1.1 \times 10^{3}$ |
| 2000 | $1.1 \times 10^{-2}$ | $6.4 \times 10^{2}$ | $1.8 \times 10^{2}$ |
| 2100 | $6.2 \times 10^{-2}$ | $1.1 \times 10^{2}$ | $3.1 \times 10^{1}$ |
| 2200 | $3.1 \times 10^{-1}$ | $2.3 \times 10^{1}$ | 6.4 |

and heat pipes could cause high $UO_2$ temperatures, but, again, this is self correcting because $UO_2$ will deposit quickly around the heat pipe and tend to bridge the area of poor contact.

The analysis that has been done to date has shown the layered fuel form to be even less sensitive to incomplete thermal contact between the core components than had been anticipated. However, it is still necessary to demonstrate that the various methods of achieving thermal contact between the molybdenum sheets and the heat pipes achieve at least 10% of full metallurgical contact. To this end finite element modeling of a sector of the reactor core is being done to determine the material motions and stresses that occur when the core is brought up to operating temperature. Concurrently, experimental measurements of temperature distributions in mock-up assemblies are being made and prototypical molybdenum sheet/heat pipe assemblies are being tested - all directed towards selecting the best method of producing the layered core configuration.

B. Joining of Heat Pipes to Core Support Plate

The basis for supporting the layered core structure is the 6-mm-thick molybdenum core support plate located where the heat pipes leave the core region. This plate must restrain the heat pipes from moving axially when the molybdenum core sheets are pushed on them during core assembly. The following attributes are desirable for the mechanism that attaches the heat pipes to the support plate:

1. It should not change the mechanical properties of the heat pipe wall, such as by reducing its thickness.
2. No welds to the wall should be used because the weld area is embrittled.
3. Weights should be kept to a minimum.
4. It should be flush with both sides of the molybdenum plate so that multifoil and the BeO wafers that bear on the plate are not interfered with.

Various attachment methods are being investigated for heat pipe/support plate junction and most take advantage of the fact that a gas-tight seal is not necessary for these joints. Direct welding of the heat pipes to the support plate is ruled out not only by the embrittlement concern, but also by the restriction of welding access by the neighboring heat pipes. The attachment methods that have been considered are illustrated in Figs. 18 to 21. Some of these have obvious shortcomings. For instance, the modified swagelok type of fitting shown in Fig. 18 results in a reduction of the heat pipe diameter that could affect the performance of some wick configurations. Initial attempts to make a swage joint with molybdenum nuts led to cracking of the nuts even though all parts were heated to 500 K, well above the ductile-brittle transition temperature of molybdenum, before torque was applied to the nuts. Tantalum nuts were tried and were successful in achieving a firm connection. The castellated nut fastener requires a groove or depression in the heat pipe wall and has been found to give a rather wobbly connection.

The use of a collar brazed or shrink-fit to the heat pipe makes possible the threaded collar and retainer ring fastening methods illustrated in Figs. 18 and 19 respectively. A molybdenum

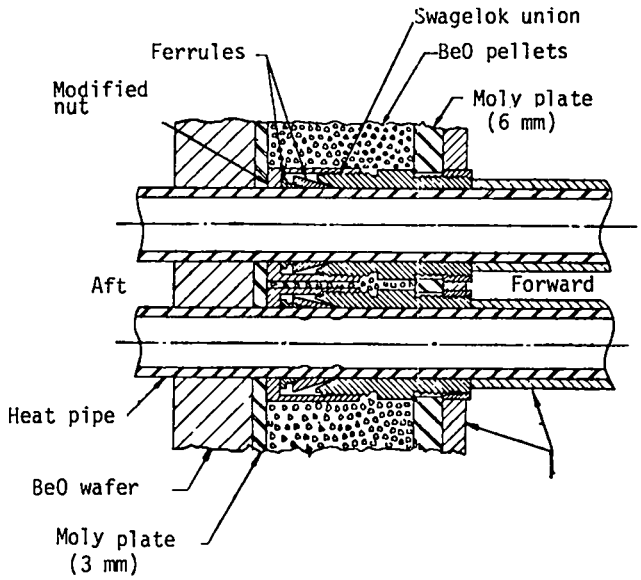


Fig. 18. Modified swagelock type fastener.

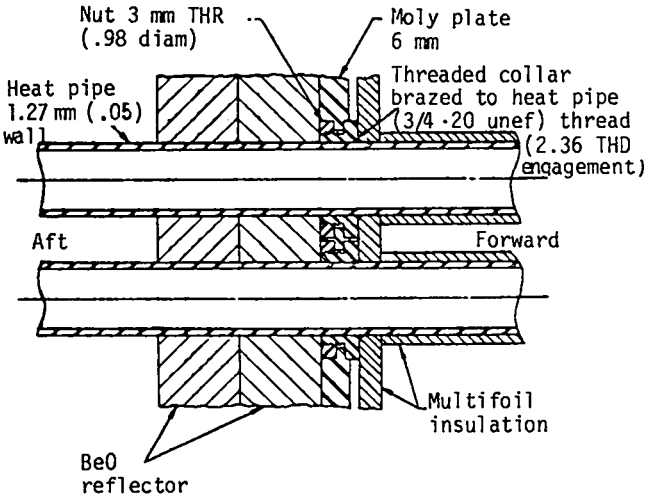


Fig. 20. Threaded collar fastener.

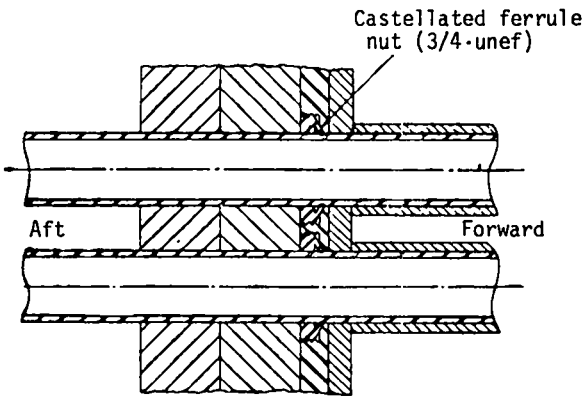


Fig. 19. Castellated nut fastener.

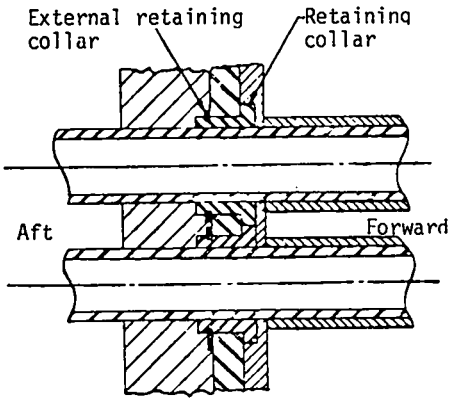


Fig. 21. Retainer ring fastener.

collar has been successfully shrunk-fit on to a 15.7-mm-diam molybdenum tube by means of the apparatus shown in Fig. 22. This apparatus holds the collar against a heated support block and aligns the tube as it is rapidly pushed through the collar for a distance of 400 mm. The trial joint was made with a collar having a 0.02-mm interference fit and was able to withstand a force of 100 N without movement. No detectable change occurred in the tube diameter.

The shrink fitting method fits all the criteria enumerated above. It is currently the favored approach for attaching the core heat pipes to the core support plate.

## C. Heat Pipe Fabrication

Three types of wick design are being investigated for use in the high-performance core heat pipes. These are shown in Fig. 23.

The screen tube configuration is the most easily fabricated, but lacks pumping redundancy and requires input heat to flow radially inward across the annular working liquid flow channel. This raises the radial temperature drop and also increases the superheating in the liquid returning to the evaporator.

The screen-covered grooved tube is highly redundant in that it retains an adequate performance margin even when several channels become inoperative. However, it also suffers the

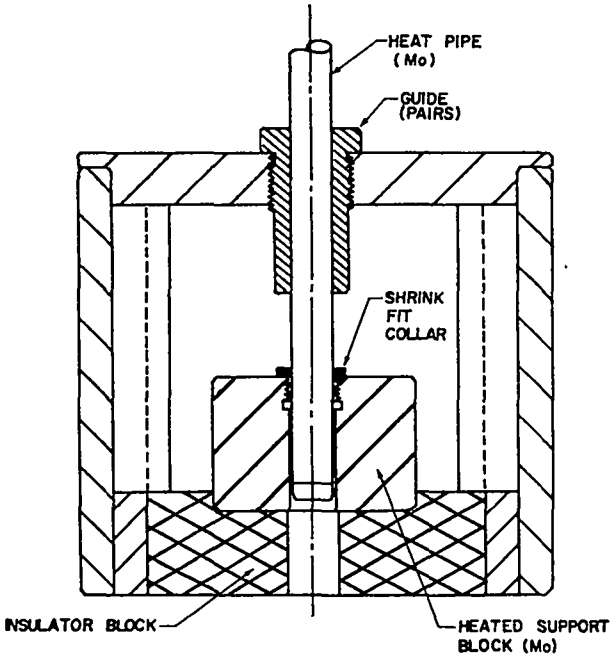


Fig. 22. Fixture for shrink-fitting threaded collar on molybdenum core heat pipe.

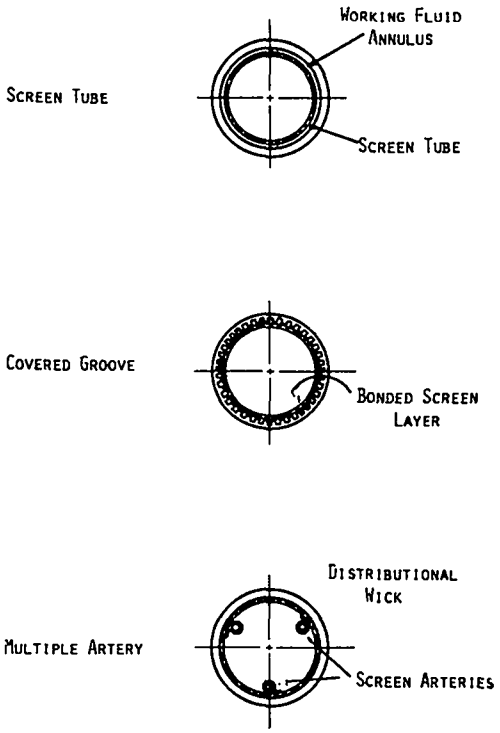


Fig. 23. Potential core-heat-pipe-wick configuration.

disadvantage of high radial temperature drop and working fluid superheating and is also difficult to fabricate.

The multiple artery configuration isolates the working liquid flow passage from the heat input, minimizing superheat and radial temperature drop. It also provides pumping channel redundancy. However, it involves a complicated fabrication procedure.

For each of these wick geometries, the pumping force is provided by the fine porosity of a multilayered screen cover. Analysis indicates that sufficient performance margin exists when the effective pore diameter of the screen is less than 40 μm. Because such fine pore size is not currently available in molybdenum screen, several forming techniques are being tried to decrease the pore size of multiple layers of the finest mesh screen that is available - 150 mesh with 25 μm wire diameter. Forming techniques used to compress the screen layers include ambient temperature pressing between hardened steel plattens to 242 and 337 MPa, rolling between stainless steel sheets, and both swaging and drawing rolls of screen between concentric low carbon steel tubes. Acid etching was used to remove the iron alloy forming or canning material and then the screen specimens were fired to either 1725 or 2025 K in hydrogen for 0.4 to 4 h. Pore diameters with the various processing techniques ranged from 24 to 80 μm. This compares with the 135 μm pore diameter of the original screen. Figure 24 shows a specimen formed between concentric tubes for which the outer tube was drawn down from 19.0 to 17.9 mm diameter. The pore diameter achieved for this specimen was 69.5 μm. Attaining finer porosity has been done at the expense of flow passage density. This can be seen in Fig. 25, which shows a specimen formed between concentric tubes by swaging the outer tube diameter from 19.0 to 12.7 mm. The pore diameter measured by a bubble breakthrough test was 23.6 μm.

It appears that the flow passage density perpendicular to the plane of the wick is sufficient for either annular wick units or arteries but there is some question whether the density of transverse flow passages is sufficient for distributional wicks. Tests are in progress to measure the flow resistance of these specimens in both directions.

In guaranteeing long life operation of the molybdenum core heat pipes, it is essential that the welding required to seal the units - both end cap and pinch off tube welding - be done so as to give

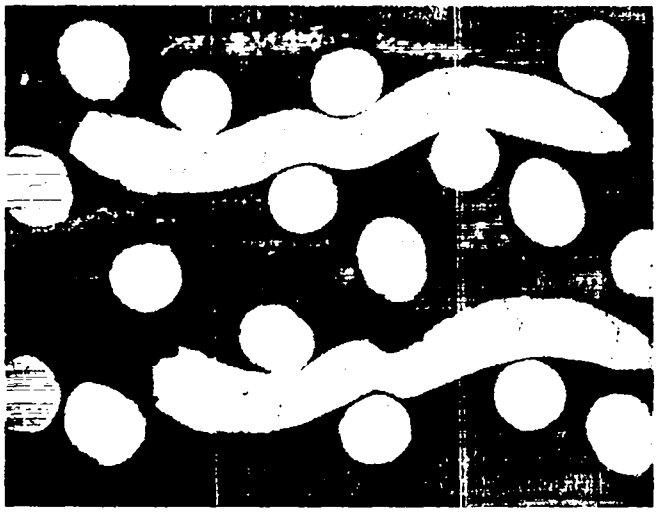

Fig. 24. Photomicrograph of 150 mesh molybdenum screen lightly compressed to give a characteristic pore diameter of 69.5 μm. Wire diameter is 50 μm.

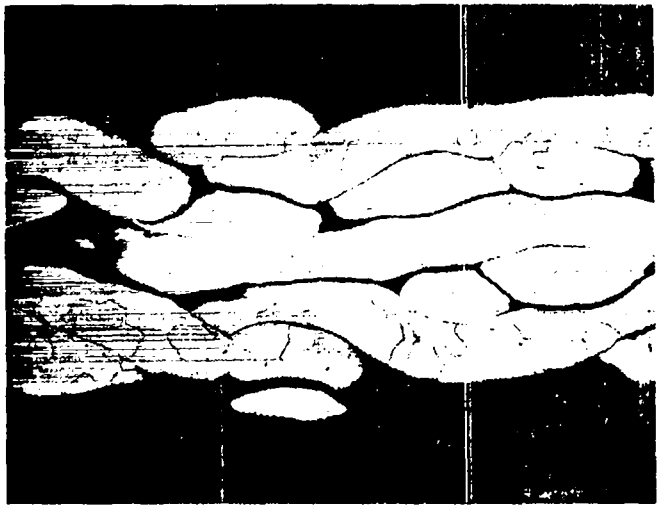

Fig. 25. Photomicrograph of heavily compressed 150 mesh molybdenum screen. Bubble point pore diameter is 23.6 μm. Initial wire diameter is 50 μm.

adequate penetration and fine grain size in the weld zone. This type of weld has been successfully made for the caps of straight heat pipes with electron beam welding techniques. However, it is more difficult to apply this method to the bent heat pipe configuration required for the SPAR power system. For this reason, some work has been initiated in looking at laser and pulsed TIG welding techniques as alternative heat pipe sealing techniques.

High-repetition rate ( > 30 pps) pulsed Nd-YAG laser welding gives a low heat input that is commensurate with the need for weld zone grain size control. Trial end cap welds were made with this method. These were not successful because the maximum penetration obtained was 1.0 mm for a joint designed for 1.5 mm. As a result, severe underfill occurred in the weld bead, resulting in extensive solidification cracking. Revision of the joint design is in process and further testing of the laser method as well as trials of the pulsed TIG method will be made.

Work has been initiated on gauging the comparative effectiveness of laser and electron beam welding for sealing molybdenum pinch-off tubes. The specific procedure involves the making of a temporary seal in a nickel or stainless steel tube that is attached to the molybdenum tube by a swage connector. A 20-mm length of the 6-mm-diam molybdenum tube is then raised to a temperature of about 550 K and flattened in a small portable hydraulic press. The final seal is made by passing a weld bead across the flattened portion of the tube. Two laser and several electron beam trials have been made on specimens of vacuum arc cast molybdenum tubing. Weld penetration problems again limited the effectiveness of the laser welding method and weld cracking occurred. Less extensive cracking was also observed on the initial electron beam welded specimens. However, changing the pre-pinch heat treatment form 1 h at 1200 K to 1 h at 1700 K has made it possible to make seal welds free of cracks and leak tight. Photomicrographs of the seal welds in vacuum arc cast molybednum and TZM tubes show the latter to look better, primarily because of small grain size in the weld bead.

D. Heat Pipe Testing

In the interval required to establish molybdenum heat pipe fabrication methods and install special fabrication equipment, work on characterizing the relative performance of the various types of heat pipe wick design and determining the effect of bends in the adiabatic section of the heat pipe has been done with stainless steel heat pipes with sodium working fluid. Performance tests of a screen tube

wick geometry have shown general agreement with the analytical predictions. The comparison is shown in Fig. 26 where the axial flow of heat per unit cross-sectional area is plotted as a function of temperature at the exit of the evaporator. The required heat transport from the reactor core of 100 $MW/m^2$ has been obtained at a temperature more than 200 K below the nominal reactor operating temperature. Measurements were not made at higher temperature for these units because of their stainless steel construction.

Another stainless steel/sodium heat pipe with a screen tube, annular wick geometry was used to investigate superheating limits. This unit was operated vertically with the evaporator at the top so that the working fluid had to flow up a gravity gradient. Under these conditions a wick dryout condition was observed at a temperature of 1200 K and a heat load of 3 KW. This dryout was assumed to be a result of runaway bubble growth in the superheated working fluid in the wick annulus. This growth comes about when a nucleation site is large enough to form a bubble of such size that the expansion force of the net pressure of the vapor within the bubble exceeds the contracting force caused by surface tension. The nucleation site diameter calculated for the observed fryout condition was 4.4 μm. This value was calculated for the heat pipe data given in Fig. 27 and is represented in the figure as a horizontal line. Figure 27 is a plot of the maximum nucleation site diameter that can be tolerated for the annular wick versus the axial heat flux limit of the heat pipe in horizontal operation. It illustrates the effect that, as the heat flux limit of the pipe is increased by operating at ever higher temperatures, the size of the tolerable nucleation site rapidly decreases. Thus, an annular wick heat pipe with the given design parameters is limited to a performance of 8.3 KW and to achieve the desired performance of ∿20 KW the maximum nucleation site diameter must be decreased from 4.4 to 0.2 μm. This can be done in principle by rigorous impurity (notably oxygen) removal methods.

The boiling limit observed in the annular heat pipe is qualitatively different for arterial wicks because the arteries are relatively isolated from the input heat flux. It is anticipated that nucleate boiling in the distribution wick could

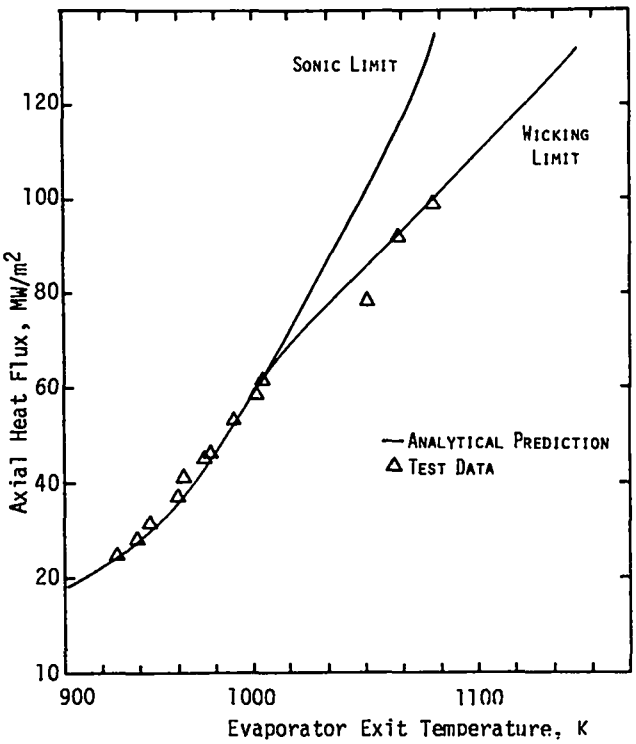


Fig. 26. Heat transport capability versus temperature for sodium heat pipe with screen-tube wick.

eventually occur to such a degree as to interfere with the circumferential flow of liquid through the wick. This phenomenon is expected to occur at much higher values of heat flux than those required for the SPAR application.

Quantitative measurements of bend effects have not as yet been completed. However, a screen-covered grooved tube with two $90^0$ bends on a 180 mm radius has been operated (in air) to 1100 K at a transmitted power density of about 4 $kW/cm^2$ - which was all that was expected for this unit based on measurements made prior to bending. This unit is shown in Fig. 28.

Although life testing of the SPAR core heat pipes with sodium working fluid is yet to commence, related data is being obtained on a molybdenum/lithium heat pipe that is being tested at 1700 K, 300 K higher than the SPAR heat pipe temperature. This unit was fabricated from low carbon, vacuum arc cast molybdenum. It contains 2 g of hafnium getter. Strips of high purity power metallurgy molybdenum are imbedded in the molybdenum wick for comparative studies. It has

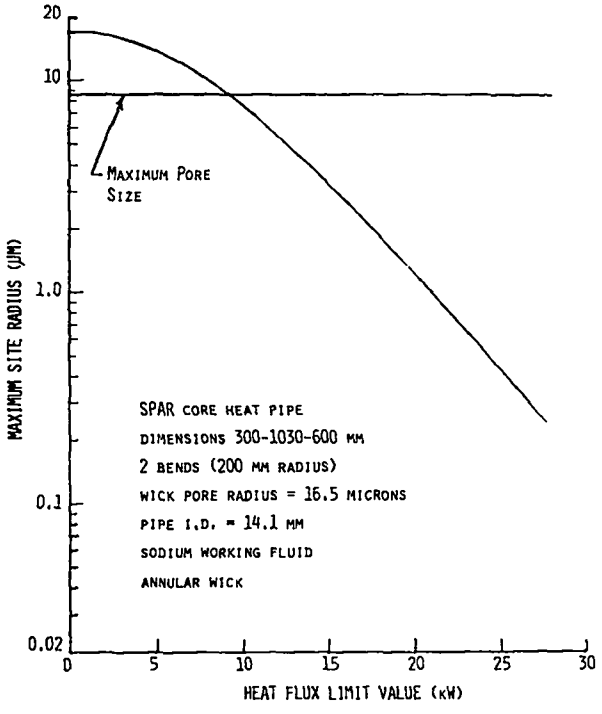


Fig. 27. Maximum tolerable nucleation site radius. for various values of the axial heat flux limit.

Fig. 28. Stainless steel heat pipe with sodium working fluid operating in air at 1100 K.

successfully withstood 78 cycles from ambient to full operating temperatures (1700 K) while accumulating 15 200 test hours.

E. Thermoelectric Material Development

Silicon-germanium alloys not only posses. attractive thermoelectric performance characteristics but also have mechanical and physical attributes that make them highly desirable candidates for space power applications. Most important of these is their stable high-temperature operating capability, because this allows higher cold-side temperatures and, hence, reduces the radiator weight of space power supplies.

The attractiveness of SiGe alloys exists despite a relatively simple lattice structure that results in thermal conductivity values considerably higher than other common thermoelectric materials and lower peak values of the figure of merit. Obviously then, a method of decreasing the thermal conductivity without changing the other physical properties that determine the figure of merit, namely the Seebeck coefficient and electrical resistivity, would yield a material of higher intrinsic efficiency. A promising approach for accomplishing such a result is to use cross-doping with Group III-V compounds to reduce the thermal conductivity of SiGe by increasing the complexity of its lattice structure. This approach is being pursued as part of the SPAR program.

The development of the cross-doping approach has been directed specifically at investigating the effect on the figure of merit of small additions of GaP to n-type 80 at.% Si - 20 at.% Ge. Specimens of this GaP-modified SiGe alloy were produced by hot pressing methods and considerable effort was devoted to optimizing fabrication parameters. Among the parameters investigated were average particle size of the starting powder, pressing temperature and pressing time.

The investigation of the effect of starting powder particle size extended over a range of 50 to 200 mesh for a 5% GaP molar concentration. Pressing parameters were 180 MPa pressure, a temperature of 1550 K and a pressing time of 1.0 h. Measurements of electrical resistivity and Seebeck coefficient over the range of 400-1000 K showed very little difference for the various starting particle sizes. The main effect was decreasing thermal conductivity with increasing mesh, presumably because the largest mesh (smallest particle size) yielded a more uniform alloy. The figure of merit versus temperature curve for the specimen made with 200 mesh, starting powder is shown in Fig. 29. This represents the best performance obtained with the 5 mole percent GaP addition.

The variation of pressing temperatures was done for a series of specimens with 5 mole percent GaP

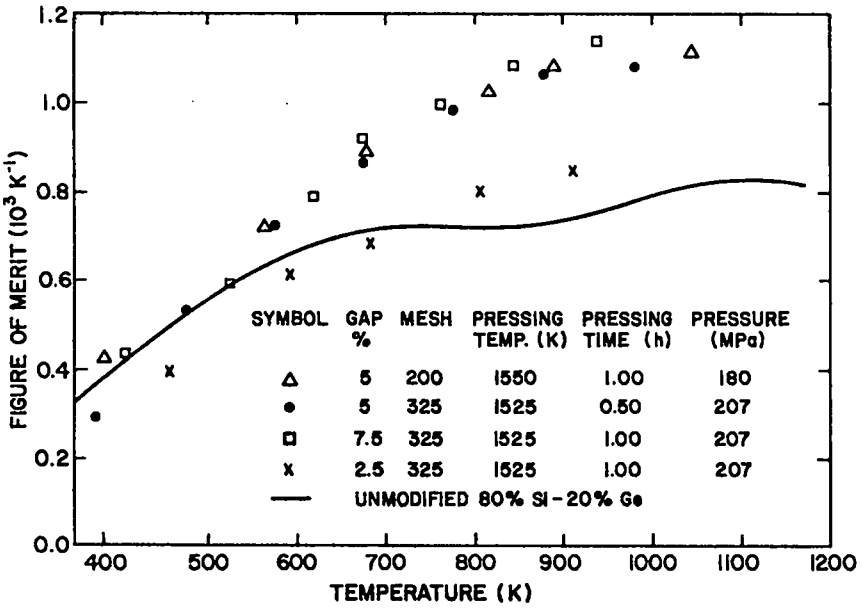


Fig. 29. Effect of GaP content on figure of merit of n-type SiGe alloy.

that were pressed at 207 MPa for 0.5 h. The starting powder particle size was chosen to be 325 mesh for this series and pressing temperatures were 1395, 1460, 1525 and 1600 K. The electrical resistivity, thermal conductivity, and Seebeck coefficient of these n-type specimens were measured as before over the 400-1000 K temperature range.

This investigation showed that the figure of merit was largest for the 1525 K pressing temperature, primarily because the thermal conductivity reached a minimum for this temperature. In order for the GaP to be effective in decreasing the thermal conductivity, it must alloy uniformly with it. It is presumed that uniformity was not achieved for pressing temperatures below 1525 K. The increase in the thermal conductivity that was observed for the specimen pressed at 1600 K is believed to result from loss of GaP occurring during pressing at this higher temperature.

A study has also been made of the effect of varying the amount of GaP added to the n-type SiGe alloy. Specimens containing 2.5 and 7.5 mole percent GaP were prepared by pressing a mixture of 325 mesh powder at 207 MPa for 1 h at 1525 K. Measurements of the figure of merit are recorded in Fig. 29 along with a solid curve giving the temperature dependence of unmodified Si-20 at.% Ge alloy. The 2.5% GaP specimen yielded a performance improvement

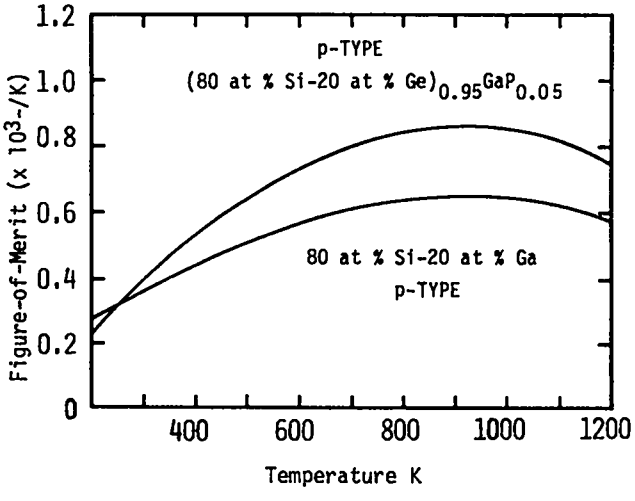


Fig. 30. Figure of merit vs temperature for p-type SiGe alloys with and without GaP additive.

over the unmodified alloy only in the temperature range above 750 K, whereas the 7.5% GaP specimen yielded the highest performance observed to date for SiGe-based alloy. In the temperature range of 750-950 K the increase in the figure of merit is 45%.

Investigations with the GaP additions to p-type Si-20 at.% Ge alloy have been limited to one run with 5 mole percent GaP. The figure of merit obtained with this material is compared to that of the unmodified alloy in Fig. 30. Above 800 K, the cold

side temperature for the SPAR system, the performance improvement is about 30%.

F. Thermoelectric Module Design

The objectives of the thermoelectric module design effort are to achieve high efficiency and low mass. The development of the GaP-modified SiGe alloy is a major step in fulfilling the first of these goals. To achieve the second, the most important step is to aim for high heat flux through the thermoelectric material because the mass of thermoelectric material required to produce a given electrical power output decreases inversely on the square of the power density. The dependence of the module mass on power density is not this strong because the relative mass of the electrical leads increases with increasing power density.

The thermoelectric module illustrated in Fig. 31 is designed for a heat flux of 500 $kW/m^2$ (50 $W/cm^2$) entering the hot side of each element of thermoelectric material. This level of heat flux input is easily achieved with the heat pipe that transmits the reactor power to the module. Less easily achieved is the thermal bonding at the interface between insulator, electrical lead, and thermoelectric material that the input heat must traverse in flowing radially through the ring segments of the thermoelectric module.

Thermal contact in the initial test mode of module segments will be achieved by using the outer sleeve of each ring segment to compress the components within, thus establishing pressure contact at the various interfaces. Figure 31 shows the design of the test model of the ring segment. Several of these units will be connected in series to form a fractional length module that will demonstrate the general feasibility of the compression module approach to high power density capability and test the effect of the thermoelectric unit load on the start-up dynamics of the heat pipe. To this end, each ring segment has its own gas gap calorimeter which can provide a close simulation of the coupling heat pipes that will encase the segments of the actual thermoelectric modules. These calorimeters are designed so that they can be installed sequentially on a cluster of closely spaced ring segments. The initial test models will be unmodified Si - 20 at.% Ge alloy thermoelectric material.

The ultimate goal of thermoelectric module development is to move to what is termed an all-bonded unit - where all the interfaces are metallurgically bonded. This approach will reduce parasitic temperature drops at the matrix interfaces to a minimum without the need for contact pressure. Creep analysis, based on silicon creep data, has shown that

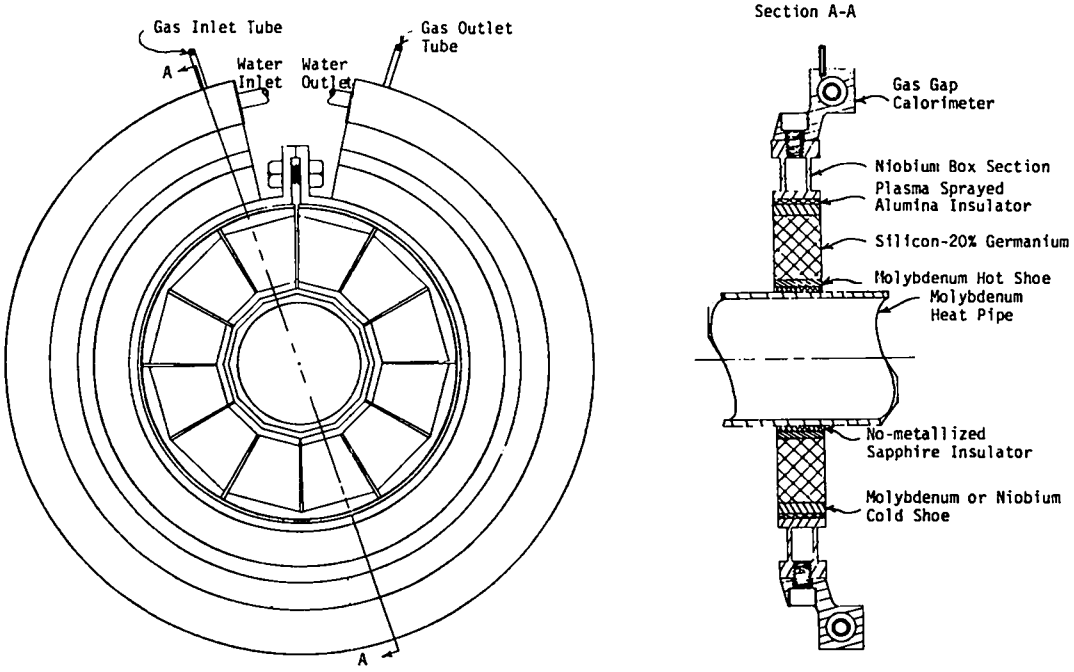


Fig. 31. Thermoelectric submodule with niobium box section and calorimeter.

maintaining interface contact pressures on the order of just a few hundred kilopascals for long periods of time is not feasible.

G. Radiator Heat Pipe Development

Because beryllium was the initial choice as the material for the radiator heat pipes, a limited effort was initiated to determine welding parameters and compatibility with nickel. The latter was of interest in case beryllium and potassium proved to be incompatible as heat pipe materials. Because nickel-potassium heat pipes have been shown to have exceedingly long lifetimes, the use of a thin layer of nickel to line the beryllium might offer a potential fix. The test of beryllium-nickel compatibility involved heating a number of samples of nickel-jacketed beryllium wire in a vacuum furnace for times up to 1373 h in the temperature range of 675 K to 975 K. Reaction layer thicknesses were determined by metallography and used to determine a reaction rate constant that is best expressed by the equation

$$Z^2 = 2.88 \times 10^{-2}\, t \exp \frac{-13,370}{T} ,$$

where Z is the layer thickness in mm, t is the time in seconds and T the temperature in Kelvin. This equation predicts a layer thickness about 0.5 mm thick would form between beryllium and nickel in a laminated heat pipe operating for seven years at 775 K. This is excessive.

Welding trials with beryllium were devoted to the problem of putting end caps on a simulated heat pipe. Both pulse TIG welding and electron beam welding methods were used on a total of four specimens. Cracking occurred in each of the trial joints. Preheating to 1035 K somewhat alleviated but did not cure the cracking problem.

The limited amount of work that was devoted to assessing the feasibility of using beryllium confirmed what was already known: that beryllium is a difficult material to work with. The recent rapid cost escalation of tubing of this material made it questionable whether it was economically feasible to use it for radiator heat pipes even if the technical problems could be overcome. This led to the elevation of titanium to the top position among potential radiator materials. Titanium has many good fabrication features, particularly welding, and its use makes possible a wide range of possible radiator heat pipe designs.

The titanium heat pipe development effort is aimed at producing thin wall heat pipes of the artery type illustrated in Fig. 32. This configuration has several advantages, one being the ease with which the arteries can be formed and securely mounted in the same welding operation that form the heat pipe envelope. The design also gives greater flexibility in the choice of a surface. The D-shaped cross section (with the flat side being the radiating surface) minimizes the amount of armor that must be used to protect the heat pipe from meteoroids. Because the armored section is of necessity relatively thick, it will have the strength, even in a flat section, to withstand buckling by atmospheric pressure. In addition the curved portion of the D-shaped cross section is much more resistant to buckling and this is highly desirable because mass minimization considerations make it desirable that its wall thickness be as thin as possible.

The D-shaped configuration also gives greater flexiblity in the choice of the distributive wick that collects the condensed fluid in the condenser section of the heat pipe and transports it to the artery and also dispenses liquid from the artery in the evaporator section. This wick can be thin layers of porous material such as screen, sintered particles or plasma sprayed material. It can also be simply a roughened surface such as made by grooving, knurling, sandblasting, differential etching or embossing. Two governing criteria in forming the distribution wick are that the effective capillary pumping radius in the evaporator be smaller than that of the artery and that this radius be sufficiently small in the condenser to wick the working fluid against gravity to a height greater than the diameter of the heat pipe so that the unit may be tested in a terrestrial environment. The former is the more stringent requirement.

Surface structuring is the favored approach of fabricating the distribution wick because it offers a smaller mass radiator system. Trials have been made with embossing, grooving, cross-grooving and sand blasting titanium sheet. Embossing is favored

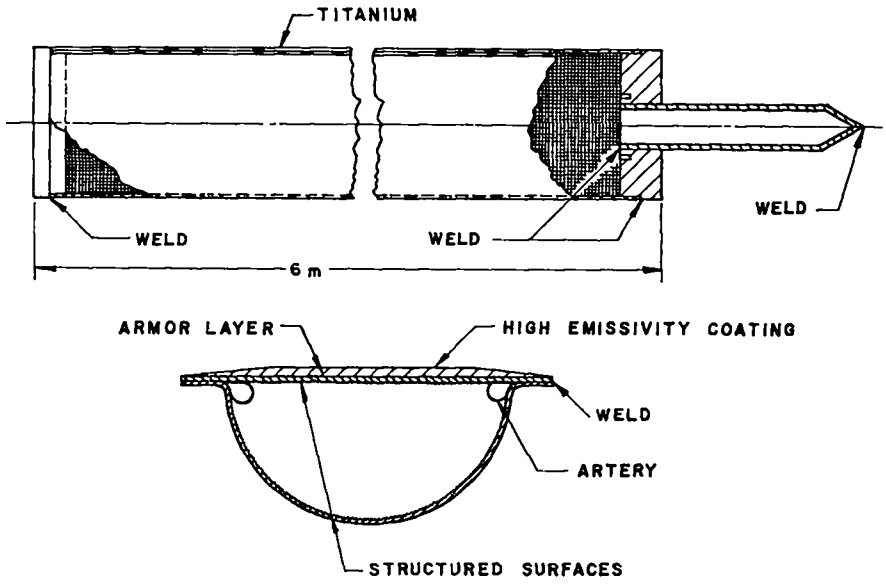


Fig. 32. Radiator type titanium heat pipe.

because of the apparent relative ease with which it can be done. However, the rolling fixture used in the initial attempts was not sufficiently heavy duty to give the desired pattern depth. Grooving and particularly cross-grooving give adequate surfaces, but are expensive to make. Wicking height measurements of sand blasted surfaces indicate they will be quite suitable for distribution wicking. The sand blasting procedure introduces extra stages of cleaning, annealing, and straightening the strips prior to forming and joining them to make the heat pipes. The first trial heat pipes of the D-configuration will use sand blasting and a combination of a sand blasted surface in the condenser and a grooved surface in the much shorter evaporator.

Tests have been initiated at the University of Dayton gas-gun facility to determine the effectiveness of titanium as an armor material. Investigations will include the study of temperature effects, oblique impacts and projective density effects. The work will also include studies of the protective value of coatings of light-weight refractory materials that can be deposited either by plasma spray or other methods to reduce the overall mass increment attributed to armor requirements.

ACKNOWLEDGMENT

This work was performed under the auspices of the US Department of Energy, Division of Advanced Nuclear Systems and Projects.

REFERENCES

1. D. Buden, "Missions and Planning for Nuclear Space Power," 14th Intersociety Energy Conversion Engineering Conference, Boston, MA, Aug. 5-10, 1979.

2. R. J. Ackerman, P. W. Gilles, and R. J. Thorn, "High Temperature Thermodynamic Properties of Uranium Dioxide," J. Chem. Phys. 25, 1089-1097 (1956).

3. W. M. Phillips and E. V. Pamlik, "Design Consideration for a Nuclear Electric Propulsion System," 13th Intersociety Energy Conversion Eng. Conf., San Diego, CA, Aug. 1978.

4. W. A. Ranken and D. R. Koenig, "Baseline Design of the Thermoelectric Reactor Space Power System," 14th Intersociety Energy Conversion Conf., Boston, MA, 5-10 Aug. 1979.

5. "Use of Nuclear Power Sources in Outer Space," Working Paper submitted by USA to Committee on the Peaceful Uses of Outer Space Scientific and Technical Subcommittee, Feb. 1979.

6. I. Bekey, A. I. Mayer, and M. G. Wolfe, "Advanced Space Systems Concepts and Their Orbital Support Needs (1980-2000)," Vols. I-IV, Aerospace report ATR-75 (7365)-1, April 1976.

Printed in the United States of America. Available from
National Technical Information Service
US Department of Commerce
5285 Port Royal Road
Springfield, VA 22161

Microfiche $3.00

| | | | | | | | | | |
|---|---|---|---|---|---|---|---|---|---|
| 001-025 | 4.00 | 126-150 | 7.25 | 251-275 | 10.75 | 376-400 | 13.00 | 501-525 | 15.25 |
| 026-050 | 4.50 | 151-175 | 8.00 | 276-300 | 11.00 | 401-425 | 13.25 | 526-550 | 15.50 |
| 051-075 | 5.25 | 176-200 | 9.00 | 301-325 | 11.75 | 426-450 | 14.00 | 551-575 | 16.25 |
| 076-100 | 6.00 | 201-225 | 9.25 | 326-350 | 12.00 | 451-475 | 14.50 | 576-600 | 16.50 |
| 101-125 | 6.50 | 226-250 | 9.50 | 351-375 | 12.50 | 476-500 | 15.00 | 601-up | |

Note: Add $2.50 for each additional 100-page increment from 601 pages up.